Available online at www.sciencedirect.com
ScienceDirect
Planetary and Space Science 55 (2007) 1069–1092
Planetary and Space Science
www.elsevier.com/locate/pss

Mercury's exosphere origins and relations to its magnetosphere and surface

F. Leblanc[a,*], E. Chassefière[a], R.E. Johnson[b], D.M. Hunten[c], E. Kallio[d], D.C. Delcourt[e], R.M. Killen[f], J.G. Luhmann[g], A.E. Potter[h], A. Jambon[i], G. Cremonese[j], M. Mendillo[k], N. Yan[a], A.L. Sprague[c]

[a]*Service d'Aéronomie du CNRS/IPSL, 91371 Verrières-le-Buisson, France*
[b]*Engineering Physics, University of Virginia, Charlottesville, VA 22904, USA*
[c]*Lunar and Planetary Laboratory, University of Arizona, Tucson, AZ 85721, USA*
[d]*Finnish Meteorological Institute, Space Research Unit, FIN-00101 Helsinki, Finland*
[e]*CETP/IPSL, 94107 Saint Maur des Fossés, France*
[f]*Department of Astronomy, University of Maryland, MD 20742, USA*
[g]*Space Sciences Laboratory, University of California, Berkeley, CA 94720, USA*
[h]*National Solar Observatory, Tucson, AZ, USA*
[i]*MAGIE, Université Pierre et Marie Curie, 75252 Paris, France*
[j]*INAF—Osservatorio Astronomico, 35122 Padova, Italy*
[k]*Department of Astronomy, Boston University, Boston, MA 02215, USA*

Accepted 9 March 2006
Available online 22 January 2007

Abstract

Mariner 10, the only spacecraft that ever passed close to Mercury, revealed several unexpected characteristics: an intrinsic magnetosphere, the highest mean density of any Solar System terrestrial planet and a very thin non-collisional atmosphere. Mercury's atmosphere is very poorly explored since only three atomic elements, H, He and O, were observed during the three flybys of Mariner 10. The measurements done by radio and solar occultations provided upper limits on the neutral and ion densities. These measurements pointed out the close connection between species in Mercury's exosphere and its surface, which is also the case for the Moon. Mariner 10 observations also characterized the vertical distributions and the day to night contrasts of Mercury's exosphere for its lightest components H and He (Broadfoot, A.L., et al., 1976. Mariner 10: Mercury atmosphere. Geophys. Res. Lett. 3, 577–580).

More than a decade later, the first observation from a ground-based observatory of Mercury's sodium (Na) exospheric component was reported (Potter, A.E., Morgan, T.H., 1985. Discovery of sodium in the atmosphere of Mercury. Science 229, 651–653). Since then, potassium and more recently calcium have been identified in Mercury's exosphere. The bright Na resonant scattering emission has been often observed since 1985. This large set of observations is now the best source of information on Mercury's exospheric mechanisms of ejection, dynamics, sources and sinks. In particular, several of these observations provided evidence of prompt and delayed effects, both localized and global, for the very inhomogeneous Mercury's Na exosphere. These inhomogenities have been interpreted as the trace of Mercury's magnetosphere–solar wind interaction and have highlighted some of the main sources of exospheric material. Some of these features have been also interpreted as the trace of a global dayside to night side circulation of Mercury's exosphere and therefore have highlighted also the relation between exospheric production and upper surface composition.

Hopefully, new sets of in situ measurements will be obtained within the next decade thanks to Messenger and Bepi-Colombo missions. Until then, ground-based observations and modelling will remain the only approaches to resolve questions on Mercury's exosphere. Mercury's exospheric composition and structure as they are presently known are described in this paper. The principal models for the main short and long times terms variations and local and global variations of Mercury's exosphere are described. The mechanisms of production and their characteristics are also given. Mercury's exosphere can also be seen as part of the coupled magnetosphere–upper

*Corresponding author. Tel.: +33 1 64 47 43 03; fax: +33 1 69 20 29 99.
E-mail address: francois.leblanc@aerov.jussieu.fr (F. Leblanc).

0032-0633/$ - see front matter
doi:10.1016/j.pss.2006.11.008

surface–exosphere system and several of the links between these elements are essential to the interpretation of most of the ground-based observations. The relation between Mercury's planet composition and its exospheric composition is also considered, as is the global recycling, sources and sinks of Mercury's exosphere.

Keywords: Mercury; Exosphere; Magnetosphere; Surface; Review

1. Introduction

The atmosphere of Mercury is very tenuous, with a pressure of a fraction of pbar (Broadfoot et al., 1974, 1976). That is, it is an exosphere with Mercury's surface its exobase or, using the name given by Stern (1999) for the Moon's exosphere, it is a surface–boundary–exosphere. It results from a complex interplay of the solar wind, its planetary magnetic field and its rocky surface. It is nearly collisionless, and is highly variable with time and space, characterized by a global asymmetry between dayside and night side and rapid temporal variations, possibly related to varying magnetospheric activity (Killen and Ip, 1999). From Mariner 10 UV measurements, and telescopic optical spectroscopy from Earth, six elements have been identified: Ca, Na, K, H, He and O (Broadfoot et al., 1976; Potter and Morgan, 1985, 1986; Bida et al., 2000). Other species are expected: e.g. H_2, OH, possibly released by impacting bodies onto water ice in craters, and noble gases, both non-radiogenic (Ne) and radiogenic (^{40}Ar, ^{129}Xe). All species representative of the surface composition, directly produced by sputtering from the regolith, should also be present (Hunten et al., 1988). Ions like Si^+, O^+, Al^+ have been observed on the Moon (Hilchenbach et al., 1991, 1993; Cladis et al., 1994; Mall et al., 1998). Volatiles are supplied by solar wind and crustal outgassing, powered by solar UV radiation, particle sputtering and/or meteoritic impact (Madey et al., 1998; Killen et al., 2001). They are lost by thermal and ion escape. Mercury's exosphere is expected to have some features in common with the lunar exosphere, due to similarities between their formation mechanisms (Killen and Ip, 1999; Stern, 1999).

The estimates of the yields for various source processes are made difficult by our ignorance of the bulk composition of the regolith, which is may be volatile-rich with respect to the lunar regolith. Several possible sources of trapped volatiles have to be considered at various time scales. On short time scales (diurnal: a few terrestrial days or weeks), a fraction of atmospheric species is expected to be adsorbed at the surface (mainly during night) and released at sunrise (Sprague et al., 1997a; Hunten and Sprague, 1997, 2002), or in response to local energetic particle precipitation (Potter and Morgan, 1990; Potter et al., 1999). On longer time scales, an important large number of sputtered particles are not directly released to the exosphere, but re-adsorbed in the regolith (Killen and Morgan, 1993a, b; Sprague, 1992, 1993; Yan et al., 2006b). Additionally, the material released by impacting meteorites might be partially retained in the regolith before being delivered to the exosphere. Finally, volatiles continuously diffusing from the deep crust, like radiogenic noble gases, might be present. On geological time scales (a few billion years), solar wind ions and solar energetic particles have been implanted in the regolith, similarly to the lunar case.

Characterizing magnetosphere–exosphere–surface processes on different bodies of the Solar System is required to better understand the Solar System evolution. On Mercury, sputtering, and other volatile production processes, are expected to imprint their signatures on: (i) the composition of the upper layers of the regolith, undergoing selective depletion of elements according to their ejection rates (Leblanc and Johnson, 2003), (ii) the composition and dynamics of the exosphere, which is also the place of a region having complex recycling through adsorption and re-emission at the surface of the regolith (Hunten and Sprague, 2002), (iii) the composition and dynamics of the magnetosphere, where species can irreversibly escape to space, at a rate which is globally proportional to the net extraction rate of species at the surface, and is therefore closely related to the composition of the regolith. Due to the large time and space variability of erosion sources (sputtering, UV flux, meteoritic vapourization, etc.), Mercury is a natural laboratory for the in-depth study of ejection processes from a theoretical, modelling and observational point of view (Madey et al., 1998; Johnson, 2002).

This paper gives an update summary of what is presently known about Mercury's exosphere. The Mariner 10 observations of H and He atoms were the first to detect the presence of an exosphere at Mercury, and are discussed in detail by Hunten et al. (1988). Many puzzles remain, and observations from Messenger and Bepi-Colombo will address them. The present paper concentrates on atoms detected from the ground that were not observed by Mariner 10, and our understanding of which stands to be greatly improved by spacecraft observations. Therefore, this paper should be considered a complement to the three following excellent reviews: Hunten et al. (1988), Hunten and Sprague (1997) and Killen and Ip (1999). It derives from an active collaboration between all of the authors as an answer to the call of opportunity for Bepi-Colombo ESA mission in support to PHEBUS (Probing of Hermean Exosphere By Ultraviolet Spectroscopy: A FUV–EUV spectrometer for the MPO Bepi-Colombo mission, PI: E. Chassefière), the selected UV spectrometer for Mercury Planetary Orbiter in Bepi-Colombo. Section 2 provides some insights on what is presently known on Mercury's exosphere, whereas Section 3 gives elements of the

mechanisms producing this exosphere. Section 4 describes what is known about Mercury's dynamics driven by the coupling with Mercury's surface and with Mercury's magnetosphere. Section 5 describes Mercury's exosphere–upper surface relations. Section 6 gives some clues on the possible sources and sinks of Mercury's exosphere on a global scale and Section 7 concludes this paper.

2. Known characteristics of Mercury's exosphere

2.1. Chemical composition

Mariner 10 made the first measurements of Mercury's exosphere during the 3 fly-bys in 1974 and 1975. The UVS discovered three constituents (Broadfoot et al., 1974, 1976). Thermal scale heights for day and night side temperatures were given: Hydrogen (d 1330 km; n 230 km), He (d 330 km, n 57 km) and marginally O (d 83 km, n 14 km). The occultation experiments put upper limits on several molecular species like CO_2. Ground-based spectroscopic observations revealed Na (Potter and Morgan, 1985, 1987, 1990, 1997a, b; Potter et al., 1999, 2006; Sprague et al., 1997a, 1998a), K (Potter and Morgan, 1986; Sprague et al., 1990; Sprague, 1992, 1993), Ca (Bida et al., 2000), and an upper limit for Li (Sprague et al., 1996b). The solar occultation experiments set a global upper limit on the total content of Mercury's exosphere as being less than 10^7 neutral particles per cm^3 at the terminator (Broadfoot et al., 1976) and Mariner 10 radio occultation an upper limit on the total electronic content in Mercury's exosphere as being less than 10^3 charged particles per cm^3 all around Mercury (Fjeldbo et al., 1976). Ground-based spectroscopic searches for emissions from neutral OH have not been successful. Another plentiful element in meteorites, *S* is also predicted to be present in Mercury's exosphere. However, because the resonance lines fall in the UV, observations from above Earth's atmosphere are required to make a search (Sprague et al., 1995, 1996a). Table 1 gives a summary of the known species and those predicted based on our current understanding of the sources and sinks. We also included some values for the associated ion species from Leblanc et al. (2004). These latter values can be compared to Lundin et al. (1997) who used a different approach estimating ion density at the surface and found 10^{-3} He^+, 0.1 O^+, 10 Na^+ and 0.5 K^+ at the subsolar point.

2.2. Vertical structure and day-to-night asymmetry

A striking aspect of the exosphere is its variability in both time and space; whether this behaviour is shared by all atoms is not known but is certainly suspected. Abundances for Na have been observed to vary from less than 10^{10} to greater than 10^{12} Na cm^{-2} (Sprague et al., 1997a; Potter et al., 1999, 2006), and imaging has revealed intermittent bright areas in both Na and K (Potter and Morgan, 1990; Sprague, 1992, 1993; Sprague et al., 1998a; Potter et al., 2006), which are discussed below in Section 2.3. The most detailed observations to date were made by Mariner 10 for H and He (Broadfoot et al., 1976, Hunten et al., 1988). Analysis and modelling of these data revealed strong differences between the day and night sides and the vertical structure. Much discussion involved the notions of thermal accommodation on the surface and desorption times for atoms to re-enter the exosphere (Smith et al., 1978; Hodges, 1979). For H and He, the thermal escape time is short as they are not bound in the low gravitational field of Mercury. Modelling and as well as Mariner 10 observations, indicate two different scale heights for these atoms and questions regarding the thermal distribution has never been adequately addressed.

The vertical structure of Na and K is quite different; they are more massive and thus require more energy for thermal escape, resulting in much smaller-scale heights (about 58 and 33 km, respectively, for the thermal components). Early on, however, it was noticed that there seemed to be a much hotter component of Na present suggested by measured wings of the Na D2 emission line (Potter and Morgan, 1987). The first measurements indicated a roughly thermal exosphere with an equivalent temperature of about 500 K but later observations with somewhat higher resolving power indicated a much hotter component of about 1000 K (Killen et al., 1999). In addition, the temperature appeared to vary with latitude (Killen et al., 1999). The same situation was found at the Moon and indeed the lunar analogy may be of help to understand Mercury's exosphere (Section 2.4). Where thermal desorption dominates, measurements indicate a significant thermal component. Where photo-desorption dominates, the atoms appear to be more energetic with a higher equivalent temperature. For K, a few measurements of this type exist and many more are needed with good measurements above the limb to discern the pattern, if any, in the variable distributions. There is also a systematic dependence on local time of day, with a maximum on the morning side and lower abundances in the late afternoon (Sprague et al., 1997a; Barbieri et al., 2004; Schleicher et al., 2004). Fig. 1 provides the first observation of the Na exosphere in absorption (Schleicher et al., 2004). This is the first time that both dawn and dusk terminators are seen simultaneously, which clearly confirms the earlier conclusions of Sprague et al. (1997a) on a strong morning/afternoon asymmetries in Mercury's Na exosphere. Potter et al. (2006) recently analysed 7 Earth years of Na observations and found that the Na emission at the dawn terminator is usually brighter than at the limb, a difference that is enhanced when the solar radiation acceleration is maximal. The Na emission at the dusk terminator by contrast appears usually less bright than at the limb.

The morning maximum is explained in terms of accumulation of atoms and neutralized ions on the cold night side, followed by a quick release of atoms from the surface as soon as sunlight hits them (Sprague et al., 1997a; Hunten and Sprague, 1997, 2002). Modelling seems to

Table 1
Known and predicted species in Mercury's exosphere

Species	Zenith column density (cm^{-2})[a]	Scale height (km)[b]	Density (cm^{-3})	Origin of the column density
H I	3×10^{9}	1160 (1330)	23,230	Measured (Mariner 10)
He I	2×10^{9}	500 (330)	6×10^{3}	Measured (Mariner 10)
He II	3.5×10^{6}	500	0.8×10^{0}	Model (Leblanc et al., 2004)
Li I	$<8.4\times10^{7}$	190	5×10^{0}	Upper limit (Sprague et al., 1996b)
Li II	7.8×10^{5}	190	2×10^{0}	Model (Leblanc et al., 2004)
C I	$<1.8\times10^{12}$	96	1×10^{4}	Upper limit (Mariner 10)
C II	3.4×10^{7}	96	5×10^{1}	Model (Leblanc et al., 2004)
N I	$<9\times10^{14}$	83	6×10^{3}	Upper limit (Mariner 10)
N II	9.6×10^{9}	83	1×10^{0}	Model (Leblanc et al., 2004)
O I	$<3\times10^{11}$	72 (83)	4.4×10^{4}	Upper limit (Mariner 10)
O II	3.4×10^{6}	72	8×10^{0}	Model (Leblanc et al., 2004)
Ne I	3.7×10^{10}	580	6×10^{3}	Killen and Ip (1999)
Na I	2×10^{11}	50	$1.7–3.8\times10^{3}$	Measured (ground based)
Na II	2×10^{9}	50	6×10^{2}	Model (Leblanc et al., 2004)
Mg I	3.9×10^{10}	290	7.5×10^{3}	Model (Morgan and Killen, 1997)
Mg II	3.8×10^{6}	290	3×10^{0}	Model (Leblanc et al., 2004)
Al I	3×10^{9}	257	654	Model (Morgan and Killen, 1997)
Si I	1.2×10^{10}	248	2.7×10^{3}	Model (Morgan and Killen, 1997)
S I	2×10^{10}	36	5×10^{3}	Model (Morgan and Killen, 1997)
	2×10^{13}		6×10^{5}	Sprague et al. (1995; 1996a)
S II	7.9×10^{9}	36	4×10^{1}	Model (Leblanc et al., 2004)
Ar I	1.3×10^{9}	29	4×10^{2}	Model (Killen, 2002)
K I	1×10^{9}	30	3.3×10^{2}	Measured (ground based)
Ca I	1.1×10^{8}	174	1.6×10^{0}	Measured (ground based)
Fe I	7.5×10^{8}	124	3.6×10^{1}	Model (Morgan and Killen, 1997)
Fe II	3.5×10^{5}	124	0.3×10^{0}	Model (Leblanc et al., 2004)
H_2	$<2.9\times10^{15}$	580	$<1.4\times10^{7}$	Upper limit (Mariner 10)
OH	10^{10}	68	1.4×10^{3}	Model (Morgan and Killen, 1997)
H_2O	$<8\times10^{14}$	65	$<1.5\times10^{7}$	Upper limit (Mariner 10)

Zenith column densities are published values whereas densities are deduced from the zenith column density and the scale height with the assumption of a barometric density distribution.

[a]In Leblanc et al. (2004), the ion species are considered to have a column density proportional to the one of their neutral parent based on $n_i/n_n = T_r/T_{photoion}$ where n_i , n_n, T_r and $T_{photoion}$ are, respectively, the ion density, the neutral density, the time that an ion spends between the altitudes z and $z+dz$ and the lifetime of a neutral particle against photo-ionization at Mercury's perihelion. $T_{photoion}$ is taken from Huebner (1992), Sprague et al. (1996b) and Molina-Cuberos et al. (2003). T_r is calculated neglecting acceleration induced by the electric field of convection (such that we obtain an upper limit for the column density close to the surface) and by supposing that the B field is radially oriented (close to the surface). Therefore the velocity of the particle, which defines T_r is the particle velocity parallel to the magnetic field vector that is the radial velocity of the parent neutral. Such velocity is of the order of the km s^{-1} (the neutral particles in Mercury's exosphere are ejected from Mercury's surface with energy of the order of the eV). dz is taken as being equal to the scale height for the neutral species.

[b]Scale height: Calculated assuming that the temperature of the gas is 500 K for the volatiles (Ar, S, Na, K, Li, H, He, O, N, C, H_2, OH and H_2O) by supposing that these species are mainly ejected by thermal desorption. We used a temperature of 5000 K for the refractory (Fe, Si, Al, Mg, Ne, Kr, Xe and Ca) supposing that these species are mainly ejected either by meteoritic vapourization (temperature of 4000 K) or by ion sputtering (temperature of 10 000 K). Same scale height for ion and neutral is assumed. For H, He, O measured scale height on the dayside are indicated into brackets.

show that the morning terminator undergoes a relatively quick depletion of Na from the surface (Leblanc and Johnson, 2003). Such models suggest that by late afternoon the surface has been depleted and the local exosphere partly ionized and swept away and maintained at some level by neutrals recycled back to the surface and released again. A global migration of the neutral exospheric particles from hot to cold surfaces, and in particular from day to night sides, would also occur. Such day to night migration of the volatiles in an exosphere and subsequent release in the early morning has been actually already observed for the lunar Argon (Ar) exosphere (Hodges and Hoffman, 1975). The dayside surface depletion is, however, probably not as intense as described in Leblanc and Johnson (2003). In particular, Killen et al. (2004) have suggested that the source rate at which atoms are replenished to the upper surface by diffusion through the grains is sufficient to maintain surface Na available for other ejection mechanisms even at the subsolar point. Thus the surface depletion of Na by thermal desorption might never be fully realized in practice.

2.3. Observed source regions and their time variability

Atoms, ions and molecules are brought to the surface or released by micro-meteoroid impact, degassing from the interior, the surface regolith, and precipitation from the solar wind (see Section 6). Ions are neutralized on contact with the surface. Release from the surface also occurs by thermal evaporation (Hunten and Sprague, 1997),

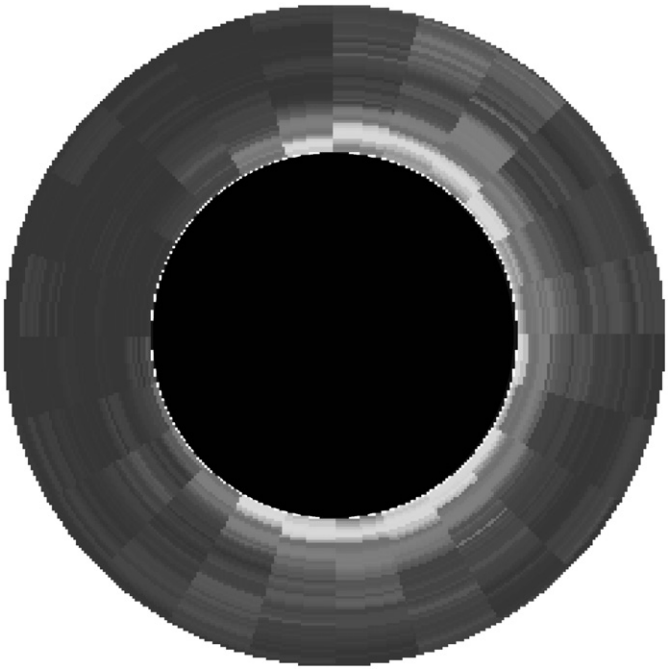

Fig. 1. Distribution of observed equivalent widths above Mercury's limb of the absorption excess by Mercury's sodium exosphere (Schleicher et al., 2004). Colours are from white to dark for the highest and smallest equivalent width of the Na exosphere. The darkest colour corresponds to the limit of sensibility of the measurement. The dawn terminator is on the right of the figure and the dusk on the left, North is at the top of the figure. Peaks of absorption can be seen at North and South high latitudes on the dawn side. Such peaks correspond to density and column density at the surface of $2.3–2.6 \pm 0.2 \times 10^3\,cm^{-3}$ and $3.0–3.4 \pm 0.1 \times 10^{10}\,cm^{-2}$, respectively. At the equator, Schleicher et al. (2004) estimated density and column density equal to $1.0 \pm 0.2 \times 10^3\,cm^{-3}$ and $1.5 \pm 0.1 \times 10^{10}\,cm^{-2}$ on the dawn terminator and density lower than $0.14 \times 10^3\,cm^{-3}$ and column density lower than $0.2 \times 10^{10}\,cm^{-2}$ on the dusk terminator. Small seeing value ($\leqslant 0.5''$) with respect to Mercury's diameter ($12''$) has been obtained thanks to Adaptive Optics. This figure is the result of 22 scans (each lasting around 18 s) obtained during the 2 h of Mercury's transit. By courtesy of H. Schleicher.

photon-stimulated desorption, PSD (McGrath et al., 1986), sputtering by impact of fast ions (Potter and Morgan, 1990), and chemical sputtering (Potter, 1995), see Section 3 for detailed information on these processes. Except for H and He and energetically ejected particles (observed for some Na and Ca atoms), most atoms execute a ballistic orbit and return to or bounce from the surface. For H and He, as many as half of the atoms thermally released from the dayside are on escaping orbits; for the non-thermal processes such as sputtering and PSD the fraction can also be large and some of the heavier atoms are on escaping trajectories.

Regions of enhanced Na and K emissions found by spectral imaging raised new questions about sources and distribution of the various components of the exosphere (Potter and Morgan, 1990; Sprague, 1992, 1993, 1998a; Potter et al., 1999, 2006). Two explanations for these bright spots have been suggested: localized ion impact leading to increased sputtering rates (Section 4.3); and source areas on the surface where Na and K have accumulated by adsorption in cold regions (Sprague et al., 1997a, Section 4.2) or by enhanced implantation (Sprague et al., 1990; Ip, 1986; Leblanc et al., 2003b). Localized ion implantation can occur in the cusps of the magnetosphere, with the location and size of the impact area being governed by the configuration of the interplanetary magnetic field (Luhmann et al., 1998; Sarantos et al., 2001; Massetti et al., 2003). The location of bright peaks at high latitudes (Potter and Morgan, 1990) and their time variability (very short with respect to Mercury's typical time scale (Potter et al., 1999) suggest the gas production by solar wind penetration into Mercury's magnetosphere and sputtering of Mercury's surface. Potter et al. (2006) concluded that excess Na emission was observed about a third of the time either in the Northern hemisphere or in the Southern hemisphere, and, more rarely, simultaneously in both hemispheres. These authors also reported no correlation with Mercury's position along its orbit or with local longitude of Mercury's surface. A second effect that can be expected, in relation to the interplanetary magnetic field, is that any change of the configuration of Mercury's magnetosphere affects the recycling rate of ions which in turns modifies the spatial distribution of Mercury's exosphere (Leblanc et al., 2003b).

One detailed modelling study predicts the content of Mercury's Na exosphere depends strongly on the true anomaly angle (TAA), the angular distance of Mercury in its orbit measured from perihelion (Leblanc and Johnson, 2003). This model predicts the total content of Na atoms in Mercury's exosphere is larger at aphelion than at perihelion, a result partially confirmed by the large set of observations by Sprague et al. (1997a). Killen et al. (2004) also compiled several years of ground-based observations of Mercury's Na exosphere and concluded that the ratio between aphelion and perihelion should be significantly smaller than predicted in Leblanc and Johnson (2003). However, they confirmed that Mercury's exosphere is probably thicker at aphelion than at perihelion. This conclusion is important since models that only account for the variations in the source and sink strengths with Mercury's heliocentric distance are inadequate. Recycling of Na from Mercury's exosphere must be included. Leblanc and Johnson (2003) show a thicker exosphere at aphelion comes from the particularity of Mercury rotation around the Sun. Its rotation is in a 2–3 resonance with its orbital motion: 87.97 Earth days, vs. sidereal rotation of 58.6 Earth days (Colombo, 1965; Colombo and Shapiro, 1966).This leads to an irregular apparent motion of the Sun as seen from Mercury's surface (Soter and Ulrichs, 1967). Such apparent motion of the Sun slows down at perihelion and even changes of direction during a short period equivalent to few Earth days around perihelion, whereas, the Sun apparent motion is significantly faster at aphelion than at perihelion. As a consequence, Mercury's night side surface, which is enriched in volatiles (see Section 2.2), moves into the dayside with a much larger speed at

aphelion than at perihelion. That is, the quantity of volatiles available for ejection into Mercury's exosphere is larger at aphelion than at perihelion and, therefore, Mercury's exospheric total content may be larger at aphelion than at perihelion.

The magnitude of the solar radiation pressure on Na atoms influences the time for thermally desorbed Na atom migration from subsolar regions to terminator regions (Smyth and Marconi, 1995) or for producing the exospheric "tail" in the anti-sunward direction (Potter et al., 2002a). Such a magnitude varies strongly with true anomaly angle (Smyth, 1986; Smyth and Marconi, 1995). Anti-correlation between radiation pressure and Na column density has been suggested by Potter and Morgan (1987) but not confirmed by Sprague et al. (1997a) using a much larger data set. Shemansky and Morgan (1991) have also suggested a significant correlation between the size of the potassium (K) column density and the solar activity, a conclusion which has been also discussed by Sprague et al. (1997a) for the Na component. More recently, Potter et al. (2006) found a significant correlation between the solar radiation pressure and the ratio of the dawn terminator Na emissions and the limb Na emissions.

2.4. What can we learn from the Moon?

The lunar exosphere exhibits many similarities to that of Mercury. Most obvious is that it has He, Na, and K as three of its constituents (Hodges et al., 1974; Potter and Morgan, 1988; Tyler et al., 1988; Kozlowski et al., 1990). A strange and unexplained matter is that H has not been detected, in spite of several efforts. It is thought that any hydrogen must be present in the form of H_2, formed from implanted solar-wind H atoms embedded in the grains of the surface and then released. However, the difference between Moon and Mercury, where H is readily detected, remains a mystery. Like at Mercury, ground-based and orbital telescopic searches have not found Mg, Fe, Si, or other constituents that might be sputtered from surface materials (Flynn and Stern, 1996; Stern et al., 1997). ORFEUS II (Flynn, 1998) detected Ar in the lunar exosphere (an observation that has been later said as untenable by Parker et al., 1998) and gave an upper limit for Neon. However, for Na and K, there is less variability and a much smaller abundance than at Mercury (Killen and Ip, 1999). After about a decade of observations of the lunar Na exosphere by a half-dozen observing groups (Mendillo and Baumgardner, 1995; Flynn and Mendillo, 1993; Mendillo et al., 1991, 1999; Sprague et al., 1992, 1998b; Stern and Flynn, 1995; Cremonese and Verani, 1997; Smith et al., 1999; Wilson et al., 2003), some badly needed laboratory work studying desorption of Na from Si substrates (Johnson and Baragiola, 1991; Madey et al., 1998; Yakshinskiy and Madey, 1999, 2000, 2001) and theoretical modelling (Stern and Flynn, 1995; Wilson et al., 1999, 2003), has lead to a general picture of what drives the lunar Na exosphere. Basically Na is released from meteoritic and surface materials as atoms (and in a lesser proportion as ions). This Na either remains in the exosphere until it is ionized or swept off the Moon into a "tail" by solar radiation pressure, or interacts with on the surface where it adsorb and desorb a number of times before sticking in cool locations. Then it is released again either thermally, around the sub-solar point where surface temperatures reach 450 K (Hale and Hapke, 2002), or by photo-stimulated desorption (sometimes called photo-sputtering, see Section 3.2). This leads to a two component, gravitationally bound quasi-thermal distribution and a more energetic escaping population (enhanced in the tail). All of these components have been observed, each by different observing techniques.

At Mercury, for Na, and possibly K, we also expect all three populations to exist. The differences in their relative abundances and physical parameters like scale height and equivalent temperature result from the higher temperatures of Mercury's surface, the greater acceleration of gravity and the intrinsic magnetic field. But great gaps in our knowledge exist with respect to H and Ca for which there is no analogy at the Moon. The ratio of the Na/K abundances in Mercury's exosphere has also been shown to be, surprisingly, very particular. The ratio has been measured as being between 20 and 140 (Potter and Morgan, 1986, 1997a; Potter et al., 2002b), whereas at the Moon it is equal to 6 ± 3 (Potter and Morgan, 1988) close to its ratio in the regolith (Stern, 1999). At Io and Europa this ratio is equal to 10 ± 3 and 25 ± 2, respectively (Brown 2001).

3. Ejection mechanisms of species at the surface

Up to now, one of the most intensively debated questions has concerned the relative importance of the different source processes for Mercury's exosphere, especially for its Na component (Fig. 2). A problem in obtaining agreement on the sources and sinks for

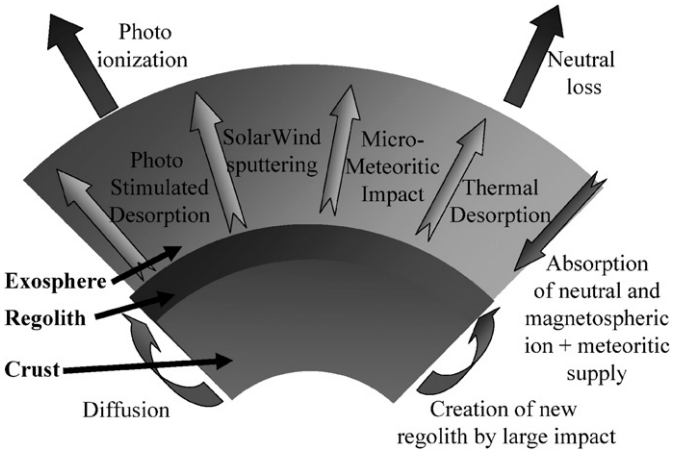

Fig. 2. Schematic view of what could be the main mechanisms acting on Mercury's exosphere. Adapted from Killen and Ip (1999).

Mercury's exosphere has been that the word source sometimes refers to the ejection process and other times for the reservoir of the Na. Here we describe the various ejection processes and use the word source for the supply of new species from the endogenic or exogenic reservoirs. Internal (endogenic) sources of exosphere must be replenished by regolith turnover, outgassing or diffusion. Recycling of locally formed ions might also be considered an endogenic source. At Mercury, external (exogenic) sources include implantation of solar ions and impacting meteoroids and comets. The ejection processes are described below and ion recycling and exogen sources are described in Section 5.

3.1. Thermal processes

At Mercury, trace atoms or molecules that are bound to or adsorbed on the surface (e.g., Ar at the Moon, Hodges and Hoffman, 1975) can be desorbed thermally (e.g., Hunten and Sprague, 1997, 2002). Whereas thermal desorption refers to ejection of a trace species, like Na at Mercury, sublimation describes ejection of the principal species. The probability per unit time, dP/dt, of ejection for thermal desorption is proportional to the surface concentration cj of a species j, to the vibrational frequency on the surface vj, and to an exponential function of the surface binding energy, Uj: e.g., $dP/dt \approx cj \times vj \times \exp[Uj/k_B T_S]$, where T_S is the surface temperature and k_B the Boltzmann constant. Thermally desorbed species that are fully accommodated have roughly Maxwellian velocity distributions, typically given as a normalized flux distribution, $f(E,\theta) = [2\cos\theta] \times [E/(kT)^2] \times \exp(-E/k_B T_S)$, where E is the energy of the desorbed particles and θ its angle with respect to the normal to the surface. Applied to Mercury's regolith, this implies that above a surface temperature of $T_S = 400\,K$ most of the Na atoms will be very quickly thermally desorbed leading to a significant surface's depletion in the early morning of Mercury (Hunten and Sprague, 2002).

This picture is, of course, oversimplified. That is, for any given species, like Na, there are a variety of binding sites (Yakshinskiy et al., 2000). Since the expression above is a probability of ejection, the shallowest binding sites are depleted first so that, in the absence of replenishment, the ejection rate can decrease with time. The time profile of this ejection is greatly modified by the distribution of surface slopes (Hunten and Sprague, 2002). There is another caveat, however, thermal annealing can change the density of binding sites and ion bombardment can produce fresh defects that act as binding sites. In addition, implanted reactive atoms, such as H from the solar wind can occupy vacated sites limiting the availability for a species that is re-adsorbed. Since the lifetime of the grain on the surface is millions of years, in the absence of sources only the most tightly bound intrinsic Na remains (Killen et al., 2004). However, Mercury's surface is constantly bombarded by micrometeorites and a major reservoir is the newly gardened material. That material is not annealed. Therefore, the question of the capability and way the upper surface reabsorbed impacting exospheric particles remain open and its answer is fundamental to solve the problem of the volatiles cycling at Mercury.

3.2. Photo-stimulated desorption/photo-sputtering

Whereas the solar photon flux heats the surface, determining the thermal desorption efficiency, individual photons can excite a bond in the surface (Madey et al., 2002). This can lead to repulsive ejection of an atom or molecule, referred to as photon-stimulated desorption or photo-sputtering. These terms have been used interchangeably but typically refer to removal of trace species vs. removal of the bulk species (McGrath et al., 1986). Stimulated desorption is less robust than thermal desorption but becomes important when the factor, $\exp[-Uj/k_B T_S]$, is small. The dominant ejecta are neutrals. Ion ejection requires deeper excitations but, since they are easy to detect, the literature is predominantly on ion desorption. Because ejected ions contribute directly to the local plasma, they might at times be important, but most observed ions are formed by photo-ionization of ejected neutrals.

Physisorbed molecular species can be desorbed by exciting internal states or by exciting a surface state (Madey et al., 2002). These can be quenched or they can lead to repulsive ejection. Exciting a surface state can lead to ejection of a molecule whereas the internal states lead to ejection of the atom pointing outward from the surface.

Adsorbed or intrinsic Na is bound in an ionic form to a silicate (Yakshinskiy and Madey, 2000). Any Na returning to the surface remains in a physisorbed state for a very short time before finding a binding site. An incident photon can excite an electron that attaches to the Na causing ejection (Yashinskiy and Madey, 1999). The threshold for desorption from a silicate or an icy surface is only a few eV (Yakshinskiy and Madey, 2001). The desorbed flux, Φj for species j, can be written as $\Phi j \approx \eta j \times \sigma j \times \Phi$, where Φ is the incident photon flux, σj is the desorption cross section, and ηj is the number per unit area in the surface. The quantity $(\eta j \times \sigma j)$ is also called the yield. Photo-stimulated desorption should be maximum at the subsolar point and larger at perihelion than at aphelion for constant ηj along Mercury's orbit (Lammer et al., 2003). The cross section σj is the product of an absorption cross section for the photon times the probability of ejection. Whereas gas-phase photo-absorption cross sections for outer shell electrons range from $\sim 10^{-17}$–$\sim 10^{-19}\,cm^2$, desorption cross sections can be an order of magnitude smaller due to the quenching of the excitations in the solid. Ejected ions can have average energies $\gg 1\,eV$ but ejected neutrals have average energies $< 1\,eV$. Stimulated desorption is non-thermal but can have a quasi-thermal component due to the interaction of the exiting atom with other surface atoms. Since planetary surfaces are porous, the ejecta often interact with neighbouring grains and, therefore, a thermal

distribution with an energetic tail is appropriate. Adsorbed water is typically dissociated by incident UV photons, electrons or ions (Johnson and Quickenden, 1997) with H or H_2 directly ejected. Due to sticking to neighbouring grains, the ejecta flux for all processes, including thermal desorption, is reduced by a factor related to the sticking efficiency and the porosity of the surface (Johnson, 1989; Cassidy and Johnson, 2005).

3.3. Charged-particle sputtering

Fast ions and electrons from the local plasma can cause desorption and sputtering by exciting the electrons, a process referred to as electronic sputtering. If the density of excitations produced near the surface is low, as is the case for incident electrons and fast protons, then electronic sputtering resembles photo-desorption (Johnson, 1990). However, the fast ions in solar energetic particle events (Leblanc et al., 2003a) can produce high excitation densities that can lead to more efficient ejection. This has not been measured for the species of interest at Mercury. Like for photo-desorption, the ejecta spectrum is not Maxwellian. It has an average energy <1 eV, but with a slowly decaying tail. A common fitting form is $f(E) \approx 2 \times E^x \times U'/(E+U')^{2+x}$, where U' is a fitting parameter, which is typically <0.1 eV, E is the energy of the ejecta and $x<1$.

The incident ions also transfer energy to surface atoms in 'knock-on' or linear cascade collisions (Johnson, 1990; Betz and Wien, 1994). This is the standard sputtering process that leads to non-selective ejection in laboratory studies. Therefore, it is a source of species other than the alkalis or volatiles such as Ar. It has been proposed to be the source of the Ca seen (Bida et al., 2000). This latter conclusion has been recently discussed in favour of ejection under molecular forms by meteoroid vapourization (Section 3.5) and photo-dissociation to form Ca atoms (Killen et al., 2005). Knock-on or linear cascade sputtering is often the dominant ejection process in most refractory solids and is most efficient at energies $\sim$0.1–1 keV amu^{-1} of the incident particles (Johnson, 1990; Betz and Wien, 1994). It has the hardest spectrum with the parameter U' above roughly related to the binding energy of the atom in the material, Uj. It is the most discussed sputtering process. Although there is a large body of data and good computational tools for knock-on sputtering, details for ejection of *trace species* from planetary materials are sparse. Therefore, one typically assumes stoichiometric ejection, which is valid if the radiation age of the material is large. That is, the sputtering rate is the rate of the erosion of the silicate matrix times the bulk concentration in stationary state (Johnson and Baragiola, 1991), or a sputtering yield is often described (the number of atoms ejected per ion incident). That is, in steady state, one uses the atomic sputtering yield of the silicate matrix times the bulk concentration. These yields also need to be corrected for the effect of sticking in the porous regolith (Cassidy and Johnson, 2005).

Typically, solar wind sputtering has been quoted as an important contributor to the high-latitude peaks in the Na emission (Potter and Morgan, 1990). Magnetospheric ion sputtering is also potentially a source of exospheric material (Cheng et al., 1987; Ip, 1986, 1987). Solar wind sputtering could contribute up to one-third to the exosphere for particular solar wind conditions (Killen et al., 2001) or in association with solar energetic particle event (Goldstein et al., 1981; Potter et al., 1999; Kabin et al., 2000; Leblanc et al., 2003a). At the Moon, ions and electrons from the solar wind, as well as from the magnetospheric lobes and plasmasheet, can all act as surface sputtering agents. These effects vary during the course of a month, and with season, as discussed recently by Wilson et al. (2005).

3.4. Radiolysis and photolysis: chemical sputtering

The incident charged particles and photons can also induce chemical processes called radiolysis and photolysis (Johnson and Quickenden, 1997). The surface is altered down to the depth of penetration by implantation of reactive species (e.g., H, C, O and S) and by bond breaking. In radiolysis and photolysis the surface material can decompose and new, more volatile species can be created which preferentially desorb changing the stoichiometry (e.g., preferential loss of O_2 from an oxide). The resulting chemical changes in the surface compete with regolith turnover and vapour deposition in determining the surface reflectance.

The chemistry produced by implanted species is often called chemical sputtering (Roth, 1983). The radiolytic processes leading to chemical sputtering consist of several steps: implantation of reactive ions, followed by chemical reactions with target atoms or molecules, and finally, desorption of the reaction products. For cases where the reaction products are volatile, the yield from chemical sputtering may be higher than for other ion-target combinations of similar mass. Sarantos et al. (2001), Massetti et al. (2003) and Kallio and Janhunen (2003b) have shown that solar wind particles will access Mercury' surface through Mercury's magnetospheric cusps when conditions of the interplanetary magnetic field are favourable (Luhmann et al., 1998). Potter (1995) suggested that solar protons impacting the surface could yield Na and water by a chemical sputtering process. The reaction of hydrogen atoms with Na-bearing silicates to yield Na atoms, water and silicon dioxide is a spontaneous process, thermodynamically favoured. Both Na and water are volatile species that could desorb from the surface. Nash et al. (1975) observed strong Na D-line emission accompanying the sputtering of various rocks by proton bombardment, consistent with the possibility of Na atom production by chemical sputtering. Potassium vapour could also be produced by chemical sputtering. Other

metallic elements (such as calcium, aluminium, magnesium, and iron) that might be produced in the surface by atomic hydrogen reactions are not sufficiently volatile to desorb from the surface, but any water produced would desorb. It should be noted that quantitative laboratory data for the efficiency of chemical sputtering by protons, needed to evaluate the importance of this process on Mercury, are not available.

3.5. Meteoroid-induced vapourization

On impact, meteoroids are vapourized and also vapourize grains in Mercury's regolith. Therefore, like knock-on sputtering it is a likely source for species other than the volatiles or semi-volatiles. Meteoroid impact has been shown to be a source of Na at the Moon (Morgan et al., 1989; Mendillo et al., 1991, 1995, 1999; Hunten et al., 1998; Verani et al., 1998; Wilson et al., 1999, 2003) and is likely important at Mercury (Morgan et al., 1988; Hunten et al., 1988; Cintala, 1992; Killen et al., 2005; Cremonese et al., 2005). These impacts also produce the porous regolith, convert surface materials into glasses, and mix the surface exposing fresh material as discussed in Section 5. The vapour is known to coat lunar grains (Hapke, 2001) and can produce a global enhancement in the Na exosphere during meteor showers at the moon (Hunten et al., 1998; Sprague et al., 1998b; Verani et al., 1998; Smith et al., 1999). Meteor showers are much less probable because very few periodic comets have their perihelion distance within Mercury's orbit. The ejecta exhibit a Maxwellian-like velocity distribution with a temperature between 1500 and 5000 K (O'Keefe and Ahrens, 1977; Sugita et al., 1998) and the amount of material vapourized per impact is of the order of a few times the mass of the impactor (Cintala, 1992). The flux of meteoroids at the surface of Mercury is usually supposed to be uniform with respect to longitude and latitude even if a parallel with the Earth's case could suggest a leading/trailing side asymmetry of the bombardment (Killen and Ip, 1999). So far only one calculation describing the characteristics of the full meteoroid flux (in term of dynamical evolution from the Earth to Mercury and vapour production when impacting) has been performed at Mercury and at the Moon for bodies having dimension between 10^{-8} and 10^{-2} m (Cintala, 1992). Vapour production rates have been recently extended to dimension up to 10^{-1} m by Cremonese et al. (2005) using Marchi et al. (2005) impacting flux for size larger than 10^{-2} m. Marchi et al. (2005) have estimated such a flux from dynamical evolution of particles (having dimension between 1 cm and 100 m, and therefore not sensible to Poynting–Robertson drag) delivered from both 3:1 and ν_6 resonances. These authors concluded that significant morning/evening asymmetries in the impacting flux at Mercury should occur at perihelion. At aphelion such a flux is roughly symmetric. Larger impact velocities are also predicted at perihelion than at any other position along Mercury's orbit.

4. Coupled exosphere–magnetosphere–upper surface system

4.1. Thermal coupling between solid surface and exospheric neutrals

Incident ions impacting the surface are implanted and, to first order, can not be distinguished from species intrinsic to the material (Madey et al., 1998). Ejected atoms and molecules returning to the surface as neutrals typically do not reflect efficiently, since their velocities are low and the surfaces are porous (Johnson, 2002). If they are re-emitted into the gas phase before fully accommodating to the surface temperature, their average energy is characterized by a thermal accommodation coefficient, $\beta = [E_{out} - E_{in}]/[E(T_S) - E_{in}]$, where E_{in} and E_{out} are the incident and re-ejection energies and $E(T_S)$ is the thermal energy associated to the surface temperature T_S (Hunten et al., 1988; Smyth and Marconi, 1995). Typically, $\beta_H = 0.08$, $\beta_{He} < 0.05$ and $\beta_{Na} = 0.62$ without consideration of porosity effect (Smyth and Marconi, 1995). Since natural surfaces are highly porous, full accommodation is a good assumption for all except the lightest atoms H and He (Hodges et al., 1974; Shemansky and Broadfoot, 1977). That is, the returning atoms or molecules become adsorbed weakly on the surface (physisorbed with a binding energy $\ll 1$ eV). In this state they can migrate along the surface of a grain until they find a deep adsorption or reaction (chemisorbed) site or they desorb thermally (Fig. 3). Therefore, with the exception of H and He, returning particles essentially stick with a residence time that depends on the surface temperature and the availability of deep sites (Smith and Kay, 1997; Yakshinskiy et al., 2000).

In laboratory studies a distinction can be made between direct reflection, sticking–migration–desorption, and sticking and becoming bound in a deep well (Smith and Kay, 1997). In modelling, one typically uses a net sticking coefficient, S, which combines the probability of physisorption and the probability of finding a binding site. For He there are no deep sites, but even Ar can bind on lunar grains. Water has a high apparent sticking coefficient on MgO, as it chemisorbs molecularly at terrace sites and dissociatively at radiation damage sites. Interestingly, the thermal activation energy in both cases is $\sim 63\,\mathrm{kJ\,mole^{-1}}$ (Stirniman et al., 1996). Yakshinskiy et al. (2000) give the net sticking for Na on a silicate: $S \approx 0.5$ at 250 K decreasing to 0.2 at 500 K. The resident time of a Na atom trapped in

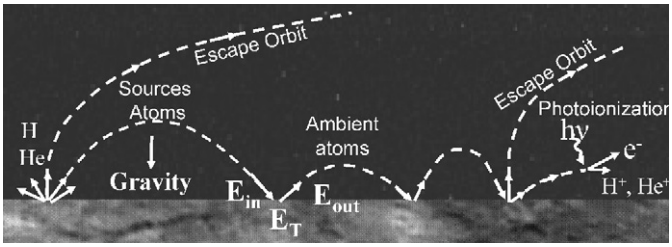

Fig. 3. Schematic view of the motion of volatiles particles at Mercury's surface. Adapted from Smyth and Marconi (1995).

a grain is expressed as $T_{Na} = 1/\nu_{Na} \times \exp(U_{Na}/k_B\ T_S)$ with $\nu_{Na} = 10^{13}\,s^{-1}$ and U_{Na} the binding energy. The binding energy of a Na atom from thin SiO_2 films has been measured recently as being between 1.4 and 2.7 eV with a most probable binding energy equal to 1.85 eV (Yakshinskiy et al., 2000). At such a binding energy and $T_S = 500$ K, T_{Na}~10 Earth hours but has been calculated as equal to 0.01 s using a lower binding energy of $U_{Na} = 1.1$ eV (Hunten and Sprague, 1997) or to 3.3×10^{-11} s using $U_{Na} = 0.25$ eV (Hunten et al., 1988).

Since the grains form a regolith, desorbed molecules intersect a surface with high probability prior to contributing to the ambient gas (Cassidy and Johnson, 2005). The atoms and molecules hopping between grain surfaces create an atmosphere in the regolith that is in equilibrium with the observed ambient gas. The effective "sticking" coefficient in a regolith is $S_{eff} \approx S/[1-(1-S)(1-P)]$, where P is the probability of escape for the regolith (Johnson, 2002). For isotropic ejection, P is ~0.2 (Johnson, 1989; Cassidy and Johnson, 2005). Therefore, at 250 and 500 K, S_{eff}~0.8 and ~0.6, close to the value found when modelling certain Na observations (Sprague et al., 1992).

4.2. Transport processes driven by Mercury's surface

Most of the neutral particles are ejected from Mercury's surface with an energy around 1 eV (see Section 3), the most energetic process of ejection being ion sputtering (up to few eVs for the largest part with a very small proportion of particles potentially ejected with higher energy by single knock-on collision, see Betz and Wien, 1994). The less energetic process of ejection is thermal desorption which ejects particles from the surface with less than 0.1 eV (~0.6 km s^{-1} for a Na atom whereas the escape velocity is equal to 4.2 km s^{-1}) at Mercury's subsolar perihelion when the surface temperature reaches 700 K (Chase et al., 1976; Hale and Hapke, 2002). Most of these particles have energy less than the escape energy (0.1 eV amu^{-1}), therefore, they follow a ballistic trajectory and reimpact the surface where they will be reabsorbed (see Section 4.1).

Such particles can again desorb, after a time of residence in the surface, unless they reach colder region where the ejection probability decreases significantly (Hunten and Sprague, 1997). Typically such regions correspond to Mercury's night side or high-latitude regions or permanently shaded regions (like interior of small craters at high latitude). These cold surfaces can act as cryogenic traps. As illustrated Fig. 4 left panel, the temperature of Mercury's surface changes dramatically going from day to night (see the scale bar). Because of the slow rotation of Mercury around itself, the temperature at the terminator decreases from 400 to 200 K in 5 Earth's days, the time for the Sun to move by 10° in longitude around Mercury. Maximum surface temperatures at the subsolar point are predicted to be equal to 510 K at aphelion (or 575 K according to Soter and Ulrichs, 1967) and to 650 K at perihelion (or 700 K following, Soter and Ulrichs, 1967) by the most recent model of Mercury's surface temperature (Hale and Hapke, 2002).

The global dayside to night side migration of the volatiles generates a strong asymmetry of the surface density between day and night sides (Fig. 4, right panel). Leblanc and Johnson (2003) using 3D Monte Carlo model found that dayside upper surface should be quickly depleted in physisorbed Na neutral particles as soon as the surface temperature reaches values $\geqslant$400 K. The discrepancy between the observation by Killen et al. (2004) and the prediction by Leblanc and Johnson (2003) discussed Section 2.3 suggests a smaller depletion of Mercury's upper surface on the dayside that is a lower efficiency for thermal desorption in depleting Mercury's upper surface than calculated by Leblanc and Johnson (2003). However, any process leading to volatiles ejection should induce a day/night asymmetry. Such asymmetry leads to a strong release of the trapped Na atoms at Mercury's early morning and to a strong morning/evening asymmetry in the Na neutral exosphere as observed by Sprague et al. (1997a), Barbieri et al. (2004) and Schleicher et al. (2004). The neutral migration from day to night sides is influenced by the solar photons which can ionize a fraction of these neutral particles or can push them in the anti sunward direction by the solar radiation pressure (Smyth, 1986; Potter and Morgan, 1987; Ip, 1990; Smyth and Marconi, 1995; Potter et al., 2006). As an example for the Na atoms, the solar radiation pressure is probably the origin of the long tail observed at Mercury (Potter et al., 2002a; Leblanc and Johnson, 2003). The ionization acts as a sink for the neutral exosphere and as a source for the magnetosphere. Both effects change by a factor 2.3 from perihelion (1.4 h photo-ionization lifetime) to aphelion (3.3 h) of Mercury and are highly species dependent (Smyth and Marconi, 1995). Such values for the photo-ionization lifetime have been re-evaluated more recently to 4.4 h at perihelion and 10.2 h at aphelion based on the observations of cometary Na tails (Cremonese et al., 1997).

In Fig. 4, right panel, the surface density is larger at high latitudes on the night side because of the ion recycling calculated using an Earth-like magnetosphere (see Section 4.4 and Leblanc et al., 2003b for detailed explanations). However, in the early morning (after the terminator), the maxima in the surface density at high latitude (black circle in Fig. 4 right panel) are formed by transport of Na atoms from equatorial regions into higher latitude regions. Indeed Leblanc and Johnson (2003) reported such maxima in the surface density ignoring ion recycling. A simple analytic formula for the surface temperature is $T_S = T_0 + T_1 \times [\cos(SZA)]^{1/4}$ where $T_0 = 100$ K and $T_1 = 500$ K at 0.35 AU. Such a formula implies that $T_S = 450$ K at SZA = 76°, or 14° after the dawn terminator on the equator. At such a longitude and ±45° in latitude (position of the black circle), $T_S = 420$ K. According to Section 4.1, the time of residence of a Na atom in Mercury's regolith is T_{Na}~607 Earth days at $T_S = 450$ K for $U_{Na} = 1.85$ eV (300 s at $T_S = 600$ K) or T_{Na}~0.2 s for $U_{Na} = 1.1$ eV or

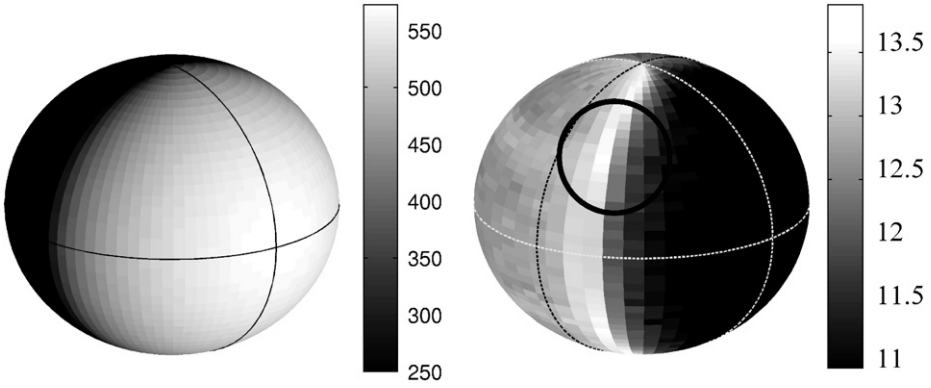

Fig. 4. Left panel: Surface temperature (K) at 0.35 AU from the Sun as seen from the morning side, assuming a smooth surface with no slope distribution (Soter and Ulrichs, 1967; Yan PhD Thesis, 2004). The limit between the dark part of the sphere (left of panel, night side) and the grey one (right of panel, dayside) is the terminator. Thin solid dark lines are for equatorial and subsolar lines. Thick dark and grey vertical solid lines are for 10° and 30° in longitude from the terminator on the dayside. Right panel: surface density distribution of the sodium absorbed atoms ($\log_{10}$ of Na cm^{-2}) when Mercury is at 0.35 AU from the Sun and as seen from the North morning hemisphere (Leblanc et al., 2003b). White lines are for the subsolar and equatorial lines. The dashed line represents the terminator. North pole is at the top of the figure.

T_{Na}~480 s for $U_{Na} = 1.4$ eV. At $T_S = 420$ K, T_{Na}~50 Earth years for $U_{Na} = 1.85$ eV or T_{Na}~1.6 s for $U_{Na} = 1.1$ eV or T_{Na}~1.8 Earth hours for $U_{Na} = 1.4$ eV. Therefore, a Na atom released at the equator can get trapped for significantly longer times at higher latitudes. These higher-latitudes region will reach $T_S = 450$ K at a longitude of 70°, that is, ~1.5 Earth days later than the equatorial regions. Another way of looking at this, during one and half Earth days, the equatorial regions will release by thermal desorption much more Na atoms than higher latitudes regions. Part of the Na atoms released at equatorial regions will get trapped in the higher-latitude regions and will accumulate for one and half Earth days.

One and half Earth days is significantly larger than the time needed for a thermally desorbed Na atom from equatorial region to reach ±45° latitudes region. The time for a pure random walk can be calculated using the method used by Hunten et al. (1988). The typical time for a hop of a particle ejected thermally from the surface is approximately equal to $2/g_M \times (k_B T_S/m_{Na})^{1/2}$, where g_M is Mercury gravitation acceleration at its surface. This is of the order of ~200 s at $T_S = 450$ K for a Na atom. A random walk of the length separating the equator from ±45° latitudes requires $(R_M/4/H_{Na}(450\,K))^2$~150 hops where $R_M/4$ is the order of the distance between equator and ±45° latitude regions and $H_{Na}(450\,K)$ ~46 km is the scale height of a Na atom at 450 K. Therefore, a Na atom will need ~8 h to move from the equator to higher latitude regions, a time which is of the order of the photo-ionization lifetime and significantly smaller than 1.5 Earth days. Here, we neglected the trapping time in Mercury's surface, as re-absorbed particles transiently occupy shallow wells. Moreover, Smyth and Marconi (1995) emphasized that random walk is not an accurate approximation for the trajectory of a Na atom around Mercury. They showed that the effect of solar radiation pressure was important and estimated the time for an ejected thermal Na atom to migrate from the subsolar point to the terminator to be between 3 and 30 h and from a longitude equal to 60° to the terminator to be between 1 and 16 h.

Due to this migration, the enriched higher latitude regions should release a larger quantity of Na atoms when they become heated than equatorial regions (Leblanc and Johnson, 2003), reproducing some of the characteristics reported during several observations of Mercury's Na exosphere (Potter and Morgan, 1990; Sprague, 1992, 1993, 1998a; Potter et al., 1999). Fig. 1 also displayed high latitude peaks in the Na exosphere on the morning side of Mercury with almost equivalent intensities. This symmetry and position of these peaks also suggests a mechanism linked to Mercury's rotation rather than a mechanism linked to solar wind penetration. The exception is in the case of a constant IMF direction during 2 h, the time length of the observation (Schleicher et al., 2004).

Anomalously radar-bright regions have been observed near the North pole (Slade et al., 1992) and near the South pole (Harmon and Slade, 1992). Such regions were later correlated with interior of small craters (Harmon et al., 1994) and their typical albedo identified as similar to water ice buried under few tens of cm of dust. The origin of these regions is thought to be H_2O or S volatiles which migrate from the dayside into these particular cold trap regions where such volatiles are stable within permanently shaded regions of Mercury's surface (Sprague et al., 1995; Killen et al., 1997). Sprague et al. (1997a) also reported correlation between peaks of the Na exospheric column density with radar-bright spots suggesting that the highly fractured terrain of such spots could be enriched in trapped Na.

Sprague et al. (1990) observed an increase by a factor 3.6 of the total content of K in Mercury's exosphere when Caloris Basin, a crater with a diameter equal to half Mercury's radius, is in Mercury's morning side (9.8 h local time). These authors suggested that such an enhancement could be due to the release of K atoms trapped in the fractured terrains that form Caloris Basin. The walls of a fractured terrain are heated only at high zenith angles.

Therefore they would release their volatiles by thermal desorption only at late Mercury's morning as observed. Sprague also suggested that the Caloris Basin may have impact melt or lava infills induced by the basin forming impact event and that these regions have high Na and K abundance. Such lavas would be feldspathoids, or alkali basalts like those suggested by Jeanloz et al. (1995). Then diffusion of the enriched material might sustain the observed enhancements. Potter et al. (1999) observed a global increase by a factor 3 (Killen et al., 2001) of the total content of Mercury's Na exosphere over a period of 7 consecutive Earth days. During this time, Caloris was moving from 7 h local time to 8.6 h local time. Killen et al. (2001) examined this data but found no evidence for an enhancement associated with the Caloris Basin. Yan et al. (2006b) recently have coupled the 3D Monte Carlo model of Leblanc and Johnson (2003) to a surface temperature model of Caloris Basin, taking into account only the effect of a sloping terrain on the solar insulation. These authors concluded that some of the characteristics of the observations of Potter et al. (1999) could be attributed to the slopes of Caloris Basin.

4.3. Solar wind interaction and magnetospheric dynamics

Magnetic and electron measurements during Mariner 10 (M10) flybys in March 29, 1974, and March 16, 1975 clearly illustrated that Mercury, like the Earth, has a bow shock and a magnetosphere (Ness et al., 1974, 1975; Ogilvie et al., 1977). Mariner 10 measurements suggested that the Hermean magnetosphere is in many respect a miniature of the Earth's magnetosphere (Ogilvie et al., 1977). The distance of the Hermean bow shock and its magnetopause was found to be reproduced from the position of the Earth's bow shock and magnetopause by scaling down their spatial distances by a factor of about 8 (see Ogilvie et al., 1977), the Hermean magnetospheric (absolute) linear dimensions being only about 5% of those of the Earth. The Mercury occupies therefore much larger fraction in its magnetosphere that the Earth in the terrestrial magnetosphere (Fig. 5).

The Hermean magnetic dipole moment has been estimated to be about 300 nT R_M^3 (R_M being Mercury's radius and equal to 2439 km), although it should be noted that M10 measurements made it impossible to determine unambiguously the strength and the orientation of the dipole moment and/or possible higher magnetic multipoles (Connerney and Ness, 1988). There are several consequences for the plasma parameters of the "miniature" size of the Hermean magnetosphere The absolute linear scale has been suggested to be a scaling factor also for dynamic magnetospheric processes. These are about 20 times faster at Mercury than at the Earth (Siscoe et al.,1975). The miniature size has also been argued to affect the plasma parameters (see, for example, discussions in Ogilvie et al., 1977). Mercury occupies such large fraction of its magnetosphere that formation of an Earth-like inner magnetosphere with a closed ring currents is not anticipated. Finite Larmor radius effects are expected to be of paramount importance at Mercury. One can also expect the loss cone of charged particles to be larger at Mercury than at the Earth.

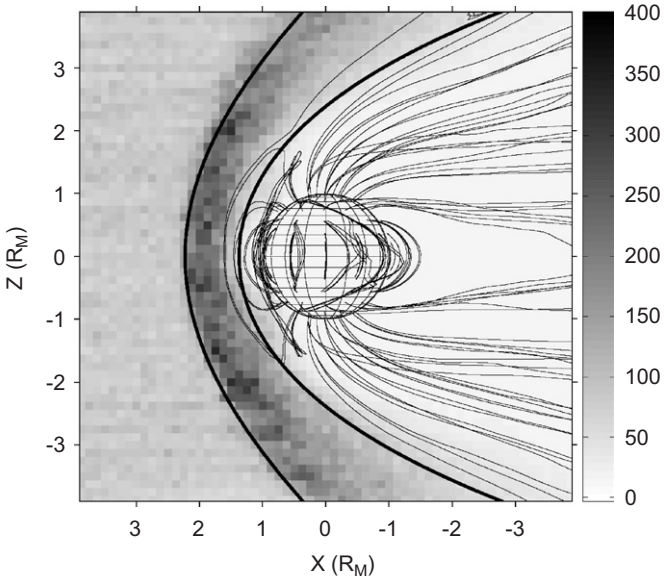

Fig. 5. Illustration of the size of the Hermean magnetosphere: plotted are the density of the solar wind protons (right scale bar in cm^{-3}) and the magnetic field lines. The solid black lines show the position of the bow shock and the magnetopause. The figure is based on a self-consistent quasi-neutral model in which the upstream parameters were IMF = [0, 0, 10] nT, the solar wind velocity of 430 km s^{-1} and the density of 76 cm^{-3} (Kallio and Janhunen, 2003b).

The scaled-down Earth magnetosphere is also expected to produce magnetospheric cusps and auroral ovals, which lie at much lower latitude than is the case at the Earth (c.f. Section 6.3). The primary reason for the smallness of the Hermean magnetosphere is its weak intrinsic magnetic field. Magnetic pressure can balance the dynamic pressure of the solar wind at only a few planetary radii from the surface (Siscoe and Christofer, 1975; Hood and Schubert, 1979; Goldstein et al., 1981). The solar wind parameters are expected to influence the characteristic features of the planet's magnetosheath and magnetosphere, especially, the connection to the IMF (Luhmann et al., 1998). The possible role of the interplanetary magnetic field IMF has been a subject of Hermean magnetosphere studies based on both analytical (Sarantos et al., 2001) and self-consistent numerical studies (Kabin et al., 2000; Ip and Kopp, 2002; Kallio and Janhunen, 2003a, b, 2004).

The self-consistent simulations have demonstrated that the weak intrinsic planetary magnetic field can result in a magnetic field morphology for which the planet can be magnetically connected to the interplanetary magnetic field, even in the case when the dynamic pressure of the solar wind is not large enough to push the nose of the

magnetopause to the surface (Fig. 6(a)). Occasionally, the pressure of the solar wind is large enough to push the magnetopause to the surface of the planet, as demonstrated by MHD (Kabin et al., 2000) and quasi-neutral hybrid models (Fig. 6(b)).

Another notable difference between the Hermean and terrestrial magnetospheres is that Mercury lacks an ionosphere (Lammer and Bauer, 1997). Hermean magnetospheric currents may thus not be expected to close above the surface, as is the case at the Earth. The method for closure of the field aligned currents, which were identified from Mariner 10 magnetic field measurements (Slavin et al., 1997), is still open.

One possibility is that the currents are closed through the planet itself (Janhunen and Kallio, 2004). How these anticipated differences at Mercury and the Earth affect the ability of their magnetospheres to store and to release energy, and their sensitivity to the upstream conditions is unclear. In addition, the Earth's ionosphere is a dense source of magnetospheric plasma that is not available at Mercury. The effect of that is not yet known.

Mariner 10 measured temporal variations that have been suggested to be caused by Earth-like magnetospheric disturbances. These variations may be strongly linked to the variations of the upstream parameters (see Section 4.5). Indeed, global simulations that have been used to study the response of the Hermean magnetosphere to the interplanetary magnetic field (Sarantos et al., 2001; Kallio and Janhunen, 2003b) suggest a strong coupling between Mercury's magnetosphere and the solar wind.

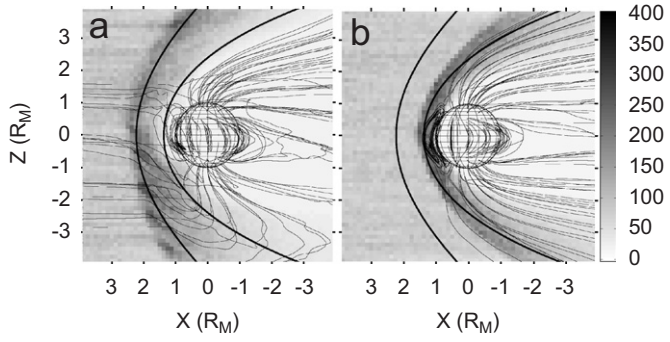

Fig. 6. Morphology of the Hermean magnetosphere (plotted are the density of the solar wind protons (right scale bar in cm^{-3}) and the magnetic field lines) in (a) the nominal Parker spiral angle case (IMF = [32, 10, 0] nT, $U_{sw} = 430\,km\,s^{-1}$, $n_{sw} = 76\,cm^{-3}$) and (b) in the high solar wind dynamic pressure case (IMF = [0, 0, 10] nT, $U_{sw} = 860\,km\,s^{-1}$, n_{sw} $76\,cm^{-3}$) based an a global model (Kallio and Janhunen, 2003b). Note how the IMF Bx component in the Parker spiral angle case results in a North–South asymmetry, the other hemisphere being magnetically connected to the solar wind, and that how the bow shock and the magnetopause are located very close to the surface of the planet at high solar wind dynamic pressure case. The solid black lines show the same bow shock and the magnetopause positions as in Fig. 5 (Kallio and Janhunen, 2003b).

4.4. Ionospheric processes, ion circulation in the magnetosphere

The scales of both the spatial and temporal field variations are much smaller at Mercury than at Earth. The first consequence of the small spatial scales at Mercury is the centrifugal acceleration that affects particle transport. Regardless of their origin (solar wind or planetary exosphere), ions travelling from high to low latitudes are subjected to enhanced outward oriented parallel acceleration due to the large curvature of the $E \times B$ drift paths. This leads to populations in the magnetospheric lobes that are substantially more energetic (typically, a few hundreds of eVs) than at Earth (Delcourt et al., 2002). Another consequence of the small spatial scales of the Hermean magnetosphere has to do with violation of the particle magnetic moment (first adiabatic invariant), most notably for ions of planetary origin that have large mass-to-charge ratios (e.g., Na^+). First-order estimates reveal that, in contrast to the Earth's magnetosphere where non-adiabaticity is only achieved beyond the essentially dipolar region (typically, tailward of geosynchronous orbit), non-adiabatic behaviour in the Hermean magnetosphere may occur in the immediate vicinity of the planet. The adiabatic or non-adiabatic character of particle motion is of paramount importance for the magnetosphere structure and dynamics, allowing for particle isotropization and injection into loss cone as well as thin current sheet formation (via coherent bunching in gyration phase) or dissipation (via pitch angle scattering). Of particular importance is the non-adiabatic regime obtained when resonance occurs between the fast oscillations about the tail mid-plane and the slow gyromotion due to the small normal field component. This quasi-adiabatic behaviour (Speiser, 1965) which is restricted to high L-shells in the terrestrial magnetosphere may be effective throughout the Hermean magnetotail. It allows for large current flow in the dawn-dusk direction as well as focused precipitation onto the planet surface which may contribute to ejection of planetary material (Ip, 1993). This precipitation is seen in Fig. 7 which shows the results of single-particle trajectory calculations for Na ions produced by photo-ionization of neutral Na exospheric atoms (Delcourt et al., 2003; Delcourt and Leblanc, 2005).

Fig. 7 displays intense ($\sim 10^6\,s^{-1}\,cm^2$) impacts of energetic (several keVs) ions within two latitudinal bands that extend over 10–20° at mid-latitudes. This feature is confirmed by hybrid simulations of ion circulation at Mercury (Kallio and Janhunen, 2003b). In Fig. 7, the poleward boundary of the precipitation bands follows is due to the large Larmor radius. It is found that ions in the distant (typically, beyond 3 planetary radii) tail intercept the dusk magnetopause in the course of their gyromotion about the small B_Z component. Such finite Larmor radius effects appear of critical importance at Mercury, hampering for instance the development of a stable ring current because of the proximity of the dayside magnetopause (e.g., Lukyanov et al., 2001). During reconfiguration of the

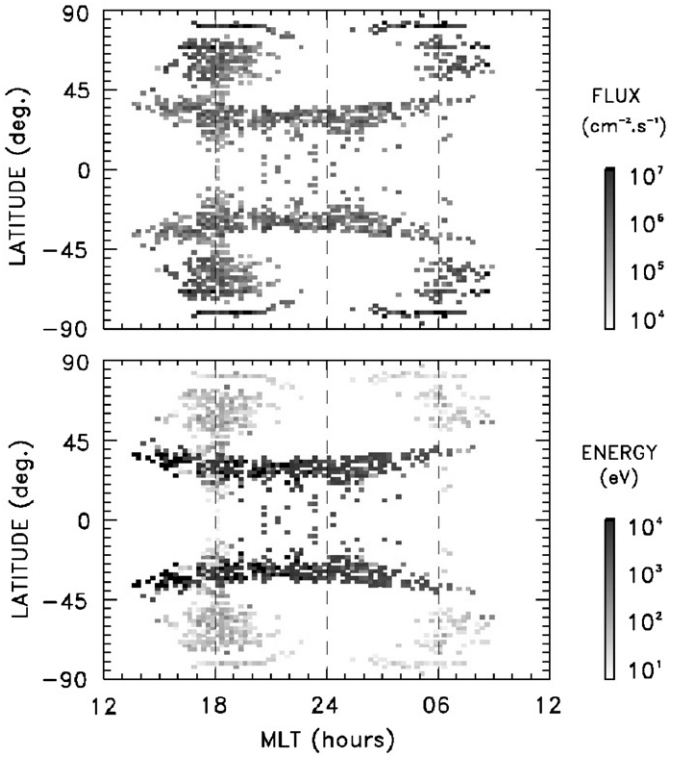

Fig. 7. Flux and (bottom panel) average energy (top panel) of precipitating sodium ions as a function of magnetic local time and latitude.

Hermean magnetosphere as a result of changes in the solar wind parameters, one expects prominent nonadiabatic transport features due to gyro-periods comparable to the field variation time scale. In this regard, Ip (1997) demonstrated that the convection surge associated with field line dipolarization, which was hypothesized from Mariner-10 data, may produce particle acceleration up to several tens of keV.

Leblanc et al. (2003b) illustrated the consequences of this, causing recycling of the Na^+ ions within the magnetosphere. These authors, using typical solar wind conditions, found enhancements in the Na emissions could be correlated to this reimplantation, which occurs in relativle narrow bands (Fig. 4 right panel, enhancement at high latitudes of Na atoms in Mercury's night side surface). They also suggested that any change in the solar wind conditions could also change the magnetospheric structure (Luhmann et al., 1998) and induce significant changes in the recycling of magnetospheric ions inducing correlated variation in the neutral exosphere.

4.5. Space weather at Mercury

On the first pass of Mariner 10 on March 29, 1974, energetic electron bursts and ULF waves were detected (Simpson et al., 1974). Flux transfer event-like features were later found at the magnetopause crossings (Russell et al., 1988), implying the existence of time-dependent reconnection processes in the solar wind interaction. All phenomena occurred more rapidly than the analogous terrestrial phenomena on Earth, consistent with expectations for the smaller-scale Hermean magnetosphere.

Many analogies were immediately noted, and continue to be made, between the observed activity and terrestrial magnetosphere substorms (Siscoe et al., 1975; Ip, 1987; Christon, 1989; Baker, 1990). However, Luhmann et al. (1998) demonstrated that the apparent substorm activity could instead have resulted from the drastic reconfigurations of Mercury's small magnetosphere in response to typical 0.3 AU interplanetary magnetic field variations compared to those occurring at Earth.

Of possibly greater importance is Mercury's magnetospheric and atmospheric response to the highly disturbed interplanetary conditions produced by solar coronal mass ejections (CMEs) such as those observed on SOHO. CMEs are eruptions of the corona that produce both solar wind disturbances in the form of a (possible) leading interplanetary shock, a period of compressed or piled up solar wind following the shock, in which solar wind density, velocity, temperature, and magnetic field are all enhanced, and a cloud of coronal ejecta, which is often characterized by a period of large magnetic field which rotated through high inclinations with respect to the ecliptic plane. These plasma and field signatures are also sometimes preceded a day or more by a burst of solar energetic particles with energies greater than several 100s of keV. A second, more intense burst of energetic ions may accompany the arrival of the shock. At the Earth, both the solar energetic particles and the plasma and field disturbance interacting with the magnetosphere produce upper atmospheric effects such as ionization anomalies, chemical changes, and auroras. What are the Hermean counterparts of Earth's "space weather" storms and their effects on Mercury's exosphere?

Some recent MHD solar wind interaction modelling (e.g. Kabin et al., 2000) and hybrid approach (Kallio and Janhunen, 2003b) confirm that a realistic enhancement of the incident dynamic pressure such as that following an interplanetary shock may render the dayside magnetosphere an ineffective shield of direct solar wind and energetic particle access to the surface. Similar conditions can result from the strong interplanetary magnetic fields associated with the CME sheath and ejecta that follow the shock, especially if the fields are southward and open up the closed magnetospheric fields via magnetopause reconnection (e.g. Luhmann et al., 1998). Under these circumstances it is possible that a solar wind sputter-dominated exosphere could exist, although a non-uniform crustal composition would still affect its spatial distribution. Potter et al. (1999) searched for a relationship between observed rapid (days) variations in the patchy Na exospheres and the occurrence of Mercury-directed CMEs observed by the SOHO spacecraft coronagraphs, with intriguing but inconclusive results. Most recently, Leblanc et al. (2003a) used a sample energetic particle event observed at Earth to estimate the effects of such an event

on the surface sputtering contribution to Mercury's Na exosphere, and concluded that fluxes several orders of magnitude larger would be required to produce Potter et al.'s inferred Na enhancements. Such events are fully within the range of variation of known solar energetic particle events. It may be that the combination of the solar energetic particle fluxes and the more open configuration of the magnetosphere during a CME-related event conspire to produce conditions where Na and other exospheric production are dominated by particle sputtering. Increased UV flux associated with a solar event was also used in the modelling by Killen et al. (2001).

5. Solid planet and its relationships with the exosphere

5.1. Solid planet outgassing

Noble gases released to the exosphere are quickly lost to space because of small gravity, high surface temperature and short ionization times. Therefore, any detection of noble gases in the Hermean exosphere would be a sign of a recent episode of outgassing, either from the eroded regolith, or originating in the mantle if volcanic gases are released from depth to exosphere through cracks. Outgassed Ar (as possibly xenon) should principally be from radiogenic origin. Indeed if Mercury is depleted in K, it should be also depleted in ^{40}Ar. If radiogenic Ar is produced by surface erosion, some correlation is expected with K, whereas if it is released by volcanic processes, decomposition products of CO_2, N_2, H_2O and other volcanic gases like SO_2 could be observed simultaneously. If Ar in Mercury's exosphere is not radiogenic, a solar wind source may be postulated.

5.2. Mineralogy and chemistry of bulk planet

Little is known about Mercury's bulk composition (Lewis, 1988). The only data available are the mean density, $5430 \pm 10\,\mathrm{kg\,m^{-3}}$ derived from mass, 0.0554 Earth mass, and radius 2439 ± 1 km. Mercury's density, which is extremely large ($5300\,\mathrm{kg\,m^{-3}}$, by correcting for self-compression and temperature effects, compared to $4100\,\mathrm{kg\,m^{-3}}$ for Earth, e.g. Spohn et al., 2001) tells us that Mercury does not have a chondritic composition and that the abundance of Fe is large with respect to other planets or to chondrites (Wasson, 1988).

Mercury's moment of inertia is among the main measurement to be done by the future space missions. From Mercury's radius, mass and expected composition, it is usually admitted that Mercury is a differentiated object. Such differentiation consists of the separation of a metallic core; the formation of liquid metal in partial melting from the residual silicate part is almost unavoidable based on the size of the parent body (Spohn et al., 2001). The product is then liquid basalt, which, because of its small density, migrates towards the surface. Mercury's core should be much larger, as compared to the whole planet, than the one of the Earth (by a factor of 2). One-half of the mass of Mercury should be contained in the core, possibly composed of pure, or nearly pure, iron. Indeed, if Mercury formed at its present place in the solar nebula, it should be depleted in sulphur and other volatiles (Lewis, 1972, 1988; Goettel, 1988). The Moon and Mercury, although of similar size, are totally different. The density and the moment of inertia of the Moon are not consistent with the existence of a significant core. The Moon has basalt seas, the most recent being $\sim$3 Gyr old. At Mercury, no direct measurement of the age of surface material exists. However, the study of the morphology of the surface shows a lack of large recent basalt seas. Mercury's tectonic activity ceased probably much earlier than on the Moon. On the Moon, an important structure corresponds to highlands formed by anorthosites. This old structure is interpreted as the product of accumulated feldspars brought to the surface by magmatic ocean in early epochs. Spectroscopic measurements strongly indicate the presence of anorthosites on Mercury (Sprague et al., 1994; Warell and Blewett, 2004). It is probable that the abundance of anorthositic structure on the Moon is related to the plagioclase stability up to a depth of 200 km (six times more than on the Earth). The equivalent value for Mercury would be a depth of 100 km for a crust of 700 km. The available aluminium concentration suggests an anorthositic crust that is likely much less than half this thickness.

We assume that Mercury is poor in volatiles (water, CO_2 and alkali metals, e.g. Lewis, 1972, 1988; Goettel, 1988), and as a consequence has a slower internal dynamic because of the larger viscosity of the mantle and because of the fact that partial melting occurs at the expected internal temperatures which are higher than those in Earth's interior. The formation of a basaltic crust enriched in radioactive elements should have induced a quick cooling of the planet.

The global composition of Mercury can be deduced, either from meteorites ejected from Mercury, or from its chondritic composition with some further assumptions. In the first case, the main difficulty is to identify such meteorites, which has not been done up to now. In the second case, the very high density of Mercury implies a probable excess of Fe with respect to chondritic composition and therefore the need of some assumption to explain such discrepancy. Among these assumptions, the loss to space of a part of Mercury's silicate due to impact at early times of Mercury's formation has been evoked as a source of strong fractionation in terms of volatiles (Benz et al., 1988; Wetherill, 1988). If a massive loss of the silicate has occured, then how would the Mg/Si ratio have changed? As a consequence, it is possible that the abundances of Al and Ca at Mercury are very large with respect to known abundances in the Solar System.

5.3. Impact history and meteoritic gardening

The meteoritic gardening and the impact history of Mercury's surface are very difficult to figure out because

the composition of the surface is not well known nor is the flux of meteoroids (Morgan et al., 1988; Cintala, 1992; Marchi et al., 2005). The very few pieces of information on the composition of the surface are due to the infrared and radio ground-based spectra and are only interpreted using strong assumptions (Vilas, 1988; Sprague et al., 1994, 1997b; Jeanloz et al., 1995; Blewett et al., 1997). Actually a highly vitrified surface resulting from impact vapourization would result in an infrared spectrum in which the absorption features are weak (Cooper et al., 2001). This is probably the case at Mercury, making the identification of surface minerals extremely difficult. If Mercury formed out of highly reduced material, the closest meteoritic analogue to surface composition would be the aubrites (enstatite achondrites) (Burbine et al., 2002). Aubrites (e.g., Watters and Prinz, 1979) are composed of essentially iron-free enstatite plus minor accessory phases such as diopside, metallic iron and sulphides. Then, the Mercury's crust would be relatively FeO-free and derived from the partial melting and recrystallization of material from the mantle. Mercury would then have formed a basaltic surface composed predominantly of FeO-poor pyroxenes (enstatite and diopside) and plagioclase. The removal of this crust would expose an enstatite-dominated mantle.

5.4. Surface charging and soil diffusion

An unexplored aspect of the alkali exosphere is the role of charging. Significant charging of the lunar grains, particularly near the terminator and on the night side has been observed (Manka and Michel, 1971). This can cause levitation of grains if the charge is large enough (Stubbs et al., 2005), but more importantly can affect the diffusion and transport of alkalis and possibly of other species within the grains (Madey et al., 1998). Early experimental work has shown that since Na is in an ionic form in most insulators, a positively charged surface can cause Na to diffuse innerward away from the surface and a negatively charged surface will enhance the diffusion of Na to the surface. Based on the lunar experience (Morgan and Shemansky, 1991), the sunlit surface is negatively charged due to photoelectron production and the night time due to flow of low energy electrons to the surface (see Jurac et al, 1995, for description of charging of grains). Unlike the moon, Mercury has plasma trapped in its magnetosphere and its flow to the surface can induce locally charging of Mercury's surface.

5.5. The genetic link between regolith and exosphere chemical composition

As explained in Section 6.2 below, a fraction of volatiles released to exosphere is thought to be meteoritic material produced by impact vapourization. On the basis of existing models, this fraction is estimated to be in the range from 10–20% to 100% (virtually no release of regolith erosion products in this case). In the second hypothesis, the composition of the Hermean exosphere reflects the chemical composition of meteorites impacting Mercury, possibly mixed with solar wind added products (see Section 6.3), and no genetic link between regolith and exosphere exists.

If only a small fraction of Mercury's exosphere is of meteoritic origin (10–20%), the rest comes from the regolith, more precisely from an upper superficial layer, an "inner boundary layer", in equilibrium with the exosphere, which may be seen as an "outer boundary layer". The interface between the regolith and the interplanetary space is due to the inner and outer boundary layers. The composition of the inner boundary layer must be significantly different from the composition of non-eroded deeper layers, due to the species dependent extraction rates. The inner boundary layer should be depleted in Na and K, more easily removed from the surface by thermal desorption and other mechanisms than, for example, calcium, which can be ejected only by the most energetic processes. In steady state, the net escape flux at the top of the exosphere is equal to the net extraction flux at the surface, which reflects the chemical composition of the unperturbed subjacent regolith. This balance between the escape flux for each species and extraction flux in steady state cannot define the abundances of exospheric species. The latter depends also on the lifetime in the exosphere, controlled by the interplay of time scales for ionization, ion re-implantation, day-to-night transport and cryo-adsorption. The outer boundary layer (exosphere) is selectively depleted in elements with high escape rates, whereas the chemical composition of the inner boundary layer is selectively depleted in elements of high extraction rates. Therefore, the composition of the bulk regolith should be better derived from the total escape rates of atoms.

6. Physical chemical cycles of volatiles at global scale

In the case of Mercury's Na exosphere, the natural choice for a system in which sources and sinks are correctly constrained (mainly based on time scale argument where the typical time scale is of the order of Mercury's day) appears to be the association between the exosphere and the upper surface in interaction with it (probably the first few meters of Mercury's surface). The sinks are essentially neutral and ion losses to space (Section 6.1). The sources of such system are then the meteoritic flux (Section 6.2), the meteoritic gardening (which is not a real source in the sense defined at the beginning of Section 3), the solar implantation (Section 6.3) and the soil diffusion (see Section 6.4).

6.1. Neutral and Ion escape/reabsorption/ionization

A fraction of the ejected neutrals has sufficient energy to directly escape Mercury gravitation. In the case of the Na atoms, this corresponds to only few percent of the total number of Na atoms ejected from the surface. For H and

He, most of the released atoms should escape. Volatiles species like N, S and O should behave roughly as the Na species whereas refractory species, such as the observed Ca, are ejected by processes that are more energetic than those for Na and K (Killen et al., 2005), resulting in a proportionately larger escape fraction. Neutral escape can also be enhanced for certain species by the solar radiation pressure.

The amount of volatiles species adsorbed within the surface layer, in particular on the night side, is basically unconstrained. From the Leblanc and Johnson (2003) model, the dayside exosphere contains 100–1000 times less Na than the night side regolith. Assuming, with Hunten et al. (1988), that the erosion rate of Mercury's regolith is $0.19\,\text{Å}\,\text{yr}^{-1}$, the production rate of Na should be only $1.1\times10^{4}\,\text{cm}^{-2}\,\text{s}^{-1}$, to be compared to the production rate of a few $10^{7}\,\text{cm}^{-2}\,\text{s}^{-1}$ currently estimated (see e.g. Smyth and Marconi, 1995; Killen et al., 2001; Leblanc and Johnson, 2003). Even if the main source of Na is infalling meteoritic matter, the net Na production rate cannot exceed $10^{5}\,\text{cm}^{-2}\,\text{s}^{-1}$ (Hunten et al., 1988). The difference by 2–3 orders of magnitude between the expected value of the production rate and the surface source rate required to explain Na observations might be explained by a net day/night exchange of Na atoms, which would undergo a great number of adsorption–desorption cycles before escaping. This factor 100–1000 is quite similar to the result of the simulation presented above. The day-to-night flux of Na atoms is obtained by multiplying the production rate by the half duration of one Mercury day (1 terrestrial month), and is of the order of $10^{14}\,\text{cm}^{-2}$. This value may be considered an upper limit, and corresponds to about a tenth of a monolayer, which may be present in the first few μm or tens μm of the regolith. Note that about the same number of adsorbed water molecules, from meteoritic origin, are expected on the base of preliminary calculations.

Moreover a fraction of the neutral particles in the exosphere can also be ionized by the solar flux. Such particles are quickly accelerated by the electric field of convection, which either puts them on an escape or re-implantation trajectories. For the Na atoms, Leblanc et al. (2003b) estimated that only 15% of the newly created ions reimpact the surface of Mercury where they are reabsorbed. Using different neutral exospheric and magnetospheric models, Killen et al. (2004) found that between 45% and 65% of the photo-ions reimpact the surface, most on the dayside and underlined the significant role of the electric field of convection in the global dawn to dusk balance of the recycled ion. In both models, the loss rate due to ion escape dominates the total loss of exospheric Na particles at Mercury. This loss rate is highly dependent on the solar wind conditions and distance to the Sun and therefore is expected to change significantly with time (Smyth and Marconi, 1995). The reimplantation of the magnetospheric ion on the surface occurs mainly in favoured regions (Delcourt et al., 2003) and could also lead to significant variation of the volatile surface concentration (Ip, 1986; Sprague, 1990) as illustrated in Fig. 4, right panel (Delcourt et al., 2003; Leblanc et al., 2003b).

6.2. Meteoritic and cometary flux

Vapour production rates depend not only on the impactor mass flux and velocity, but also on the porosity, density, and the rock types of impactor and target, respectively. Methods of calculating impact vapour yields range from simple impedance matching techniques (Morgan et al., 1988), calculations of phase changes by determining the entropy at each shocked state on a Hugoniot (the locus of possible shocked states) (Cintala, 1992), or using more elaborate hydrodynamic codes (e.g. O'Keefe and Ahrens, 1977; Pierazzo and Melosh, 1999). Although, the approaches vary widely in method and complexity, the results agree within a factor of 4–5. Additional uncertainty arises because the impactor flux at the orbit of Mercury is not well known. However, a factor of 5 difference is large enough that conclusions concerning the fraction of the exosphere supplied by impact vapourization range from about 10% to 20% (Killen et al., 2001) to near 100% (Morgan et al., 1988). Although variations in the impact-generated lunar exosphere may be caused by meteor showers (Barbieri et al., 2001; Hunten et al., 1998; Smith et al., 1999; Verani et al., 2001), it is less likely that Mercury will be impacted by periodic meteor showers since the perihelia of most of the known periodic comets are greater than 0.46 AU.

The rate of meteoritic vapourization of a regolith depends on the volume density of meteoritic material in space at Mercury's orbital distance, the velocity distribution of the meteoroids, Mercury's mass, orbital velocity, regolith density and porosity, and the meteor density and porosity. The density of meteoritic material in space at Earth orbit has been measured by the Long Duration Exposure Facility to be $3\times10^{-16}\,\text{g}\,\text{cm}^{-3}$ (Love and Brownlee, 1993) and can be scaled to orbital distance, R_{orb}, as $R_{\text{orb}}^{-1.3}$ (Morgan et al., 1988; Cintala, 1992). The mass density measured by the Long Duration Exposure Facility includes the mass in the range 10^{-9}–$10^{-4}\,\text{g}$; an equal amount is assumed to be in the 1 cm to 10 km size range (Ceplecha, 1992).

The meteoritic flux at the heliocentric distance of Mercury depends also on the particle size, as different sizes follow different dynamical paths (Marchi et al., 2005). Meteoritic sizes smaller than about 1 cm are dominated by the Poynting–Robertson effect and the estimates of the flux should be good. Larger particles have a completely different dynamical evolution. Most of them arriving on the terrestrial planets come from two important resonances located in the asteroid main belt (the resonance 3:1 with Jupiter and a secular resonance with Saturn). Recent estimates of the vapour produced by meteoroid impacts have been reported by Cremonese et al. (2005). These estimates reproduced the Cintala (1992) distribution for

particles smaller than 1 cm and they adopted the Marchi et al. (2005) distribution for larger particles. They have found an upper limit to the production rate of neutral Na atoms of 3.15×10^{24} atoms s^{-1}. This is one order of magnitude greater of what Leblanc and Johnson (2003) used. They included the meteoroid and regolith grain vapourization assuming the same composition for both. This new estimate suggests that the meteoroid impacts might be a dominant mechanism. Leblanc and Johnson (2003) suggested it could contribute up to 30% of the total production rate of Mercury's Na exosphere.

6.3. Solar wind addition

Ion impact at Mercury has been a subject of several analyses motivated by Mariner 10 (M10) magnetic field and electron measurements made in 1974–1975. However, there are no direct ion measurements available from M10 flybys. Quantitative analysis of the Hermean ion environment studies have focused on analysing the motion of ions in the Hermean magnetosphere. These are either formed from neutrals emitted from the surface and ionized in the exosphere (Delcourt et al., 2002, 2003; Killen et al., 2004; Mura et al., 2005) or from the solar wind particles injected from the tail (Lukyanov et al., 2001) or from energetic particles during Solar Energetic Particle (SEP) event (Leblanc et al., 2003a, Section 4.5). The role of the solar wind ion sputtering has received recent interest as a candidate to explain the rapid temporal variations in the Hermean Na exosphere observed in Earth-based remote sensing measurements (Potter et al., 1999; Killen et al., 2001).

Fig. 8 gives a three-dimensional (3D) view of the particle flux of the solar wind protons at the surface of Mercury based on a global model in two upstream cases: (a) when IMF has only z component and (b) when the solar wind dynamic pressure is high. The figure suggests the formation of three different high impact regions on the surface: (1) "auroral" impact on the equatorward side of the open/closed field line boundary, (2) "cusp" impact on the dayside in the noon midnight meridian plane, and (3) "nose" impact around the subsolar point with high solar wind dynamic pressure.

The impact of the solar wind proton in the auroral region shown in Fig. 8(a) is anticipated to take place at Mercury by analogy with the Earth's auroral precipitation (Ogilvie et al., 1977). Increasing the solar wind dynamic pressure pushes the magnetopause toward the planet (see 4.3, Fig. 6(b)) resulting an intense H^+ ions impact near the subsolar point (Fig. 8(b)). Furthermore, the orientation of the IMF affects the morphology of the Hermean magnetosphere and the H^+ impact flux. The North–South asymmetry in the Hermean magnetic field caused by the IMF Bx component (Sarantos et al., 2001; Kallio and Janhunen, 2003b) resulted in a North–South asymmetry also in the flux of impacting solar wind protons. The total H^+ ion particle flux is higher on the hemisphere that is magnetically connected to the solar wind (Fig. 8(a)) than in the opposite hemisphere.

The implantation of the different populations reimpacting the surface can be inferred from what we know about the Moon. Exospheric neutrals are re-adsorbed in the surface layers, as discussed elsewhere. The next largest population is made up of exospheric neutrals that are ionized and are picked-up and re-impact the surface (Section 4.4). These are mostly ions of the desorbed volatiles with some refractory species. At the Moon the solar wind fields accelerate the newly formed ions but at Mercury these are typically referred to as magnetospheric ions. Solar particle and those magnetospheric ions which impact the surface with few keVs are implanted in the grain to typical depths ~100 nm. The most energetic particles which impact the surface with more than 100 keVs can be implanted to depths up to ~100 μm.

6.4. Cycling of exospheric volatiles through the thermally forced regolith

Sprague et al. (1990) observed a significant increase in Mercury's total K exospheric content (by a factor 3.6) when Caloris Basin was in Mercury's early morning (also Potter et al., 1999, see Section 4.2). These authors explained this increase by the highly fractured surface of Caloris Basin leading to cold trapping of the volatiles of Mercury's exosphere, and their release only at late morning. As discussed earlier, this interpretation has been criticized by Killen and Morgan (1993b) who argue that diffusion rates and estimates of connected pore volume used by Sprague et al. (1990) were too large. The role of Caloris Basin has been recently reanalyzed by Yan et al. (2006b) taking into account only the role of the slope of the basin. These authors concluded that such 3.6 times increase cannot be due to the slopes of Caloris Basin.

However, diffusion through a porous regolith could play a significant role in the diurnal cycle of Mercury's exosphere. Indeed the particular astronomical parameters of Mercury's orbit induce strong temperature variations in the upper meters of Mercury's surface (Ledlow et al., 1992; Yan et al., 2006a) as illustrated in Fig. 9. As shown by Yakshinskiy et al. (2000), as soon as a grain reached temperature higher than 400 K, most of the Na atoms trapped in the surface layers of the grain are quickly released. On the dayside, an atom which reimpacts the surface, will be then released very quickly because of the high surface temperature (see Fig. 4(a)). It can be either ejected upward into the exosphere or downward through cracks deeper inside the surface. Such particle can eventually reach regions where the temperature is significantly lower than at the surface (see Fig. 9 at 10 cm depth) and therefore remains trapped below the surface even if the surface temperature is high. On the dayside, the residence time of a volatile particle with respect to depth will change with the local time and the slow motion of the heat wave into the surface.

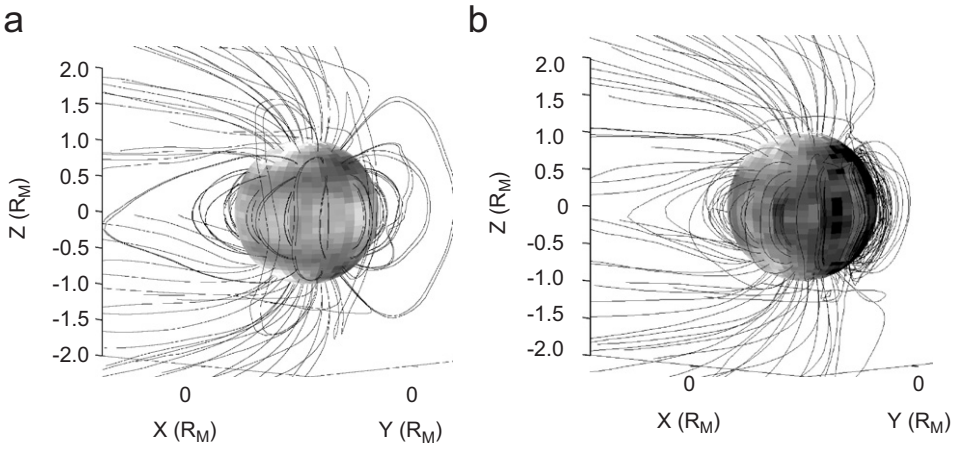

Fig. 8. Three-dimensional view of the flux of the impacting solar wind protons at the surface of Mercury and the magnetic field lines in the (a) pure northward IMF, and (b) in the high U_{sw} cases. Note the intense "auroral" impact regions around the magnetic poles, the "cusp" impact near the noon-midnight meridian plane in (a), and the "nose" impact in (b). The total impact rate of the solar wind protons in Figure a (Figure b) is ~5% (~25%) of the impact rate that would take place without the shield of the magnetosphere. The colours at the surface of the planet show the particle flux of impacting H^+ ions. Darkest to whitest colours correspond to highest and lowest flux, respectively. The values are calculated from a quasi-neutral hybrid model (Kallio and Janhunen, 2003b).

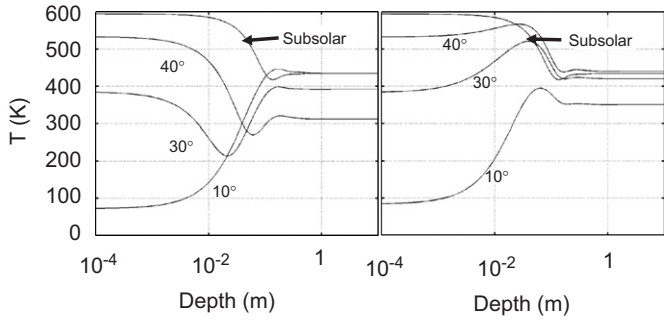

Fig. 9. Temperature within the first few meters of the upper surface of Mercury at perihelion and at the equator. Right figure: Morning side. Left figure: Afternoon side. The numbers indicated on each figure indicates the position of the point at the surface where has been calculated this profile: namely, 10° for 10° in longitude (increasing with Mercury's rotation) before the dawn terminator (left figure) and after the dusk terminator (right figure), 30° for 30° in longitude after the dawn terminator (left figure) and before the dusk terminator (right figure), 40° for 40° in longitude after the dawn terminator (left figure) and before the dusk terminator (right figure). Subsolar is for subsolar longitude (Yan et al., 2006a).

In the morning when the surface temperature increases, the volatiles are expected to slowly move in average inside the surface. With increasing solar illumination, the heat wave moves slowly downward (see Fig. 9) and should release a fraction of the volatiles, which have been trapped at depth. On the night side, because the temperature of the regolith is higher than the surface temperature (see dark lines in Fig. 9), the volatiles trapped at depth should move up to the surface of the regolith. This change in the trapping capability of the surface with time will change the reservoir of volatiles, which can be ejected into the exosphere and therefore could have potentially significant effect on the global shape of the exosphere.

7. Conclusion

More than 30 years after the only visit of a spacecraft (Mariner 10 made three flybys in 1974 and 1975), Mercury is going to be the object of two major space missions: Messenger a US single spacecraft, discovery mission which has been launched mid-2004 (Gold et al., 2001; Santo et al., 2001; Solomon et al., 2001), and the second Bepi-Colombo, an ESA corner stone mission composed of two spacecrafts, which should be launched in 2013.

The first reason for this remarkable interest of the scientific community to Mercury is that Mercury being the closest planet to the Sun, it is thought to be a key element to better understand the origin of the Solar System (Solomon et al., 2001). In particular, Mariner 10's few observations have revealed the presence of an unexpected strong intrinsic magnetic field and have confirmed the very high ratio of metal to silicate, leading to several key questions on Mercury's accretion processes, interior cooling and geological evolution.

Moreover, Mariner 10 detected only a few elements in Mercury's exosphere, namely atomic H, He and O (Broadfoot et al., 1976). Mariner 10 revealed also indicated that the total content of the exosphere was less than 10^7 neutral particles per cm^3 (Broadfoot et al., 1976) and less than 10^3 charged particles per cm^3 (Fjeldbo et al., 1976). The day to night distributions and vertical distributions of H and He have also been measured and analysed (Smith et al., 1978; Hodges, 1979; Hunten et al., 1988). In 1985, Potter and Morgan reported the first observation of the Na emission in Mercury's exosphere. Following this observation, a second new element K was detected in Mercury's exosphere (Potter and Morgan, 1986). Fifteen years later, a third element has been discovered in

Mercury's exosphere, the calcium atomic species (Bida et al., 2000).

The Na component is the most frequently observed element at Mercury. The large set of observations of Na (see Sections 2.1–2.3) has highlighted several aspects of Mercury's exosphere. It has led to an exploration of the main mechanisms of production of the Na exosphere, namely thermal desorption, photon stimulated desorption, particle sputtering, meteoroid vapourization and chemical sputtering (Section 3). Such observations also suggested a close relationship with Mercury's magnetosphere through solar wind penetration along open magnetospheric field lines, subsequent sputtering of Mercury's surface leading to remarkable features in Mercury's exosphere (Potter and Morgan, 1990). Energetic solar events have been very early identified as being potentially strong enough to compress Mercury's magnetosphere to its surface (Goldstein et al., 1981). Planetary ion recycling via Mercury's magnetosphere and solar absorption has been also often suggested as important processes in the formation of Mercury's exosphere (Section 4). At the end, such observations emphasized the role of exospheric neutral recycling from hot to cold surfaces, a process which can be related to several observed features in Mercury's Na exosphere (Sprague et al., 1997a).

It is now obvious that ground-based observations have been an unexpected and useful source of information on Mercury's exosphere. It is both necessary and likely that before the first flyby of Messenger in 2009, a large and new set of ground-based observations will be available which help guide the first measurements of Messenger and Bepi-Colombo. As an example, long and short time variability of Mercury's Na exosphere have been an unprecedented guide to better understand the dynamics of Mercury's exosphere (Sprague et al., 1997a, b; Potter et al., 1999; Killen et al., 2001, 2004). A new set of such observations are definitively needed and should be able to confirm aspects of certain models and thereby help us understand the origins of several observed features in Mercury's exosphere.

Mercury's exosphere is the main source of magnetospheric ions. Therefore, its characteristics will be essential to understand the dynamics of Mercury's magnetosphere. Mechanisms of depletion and enrichment of Mercury's upper surface can be directly related to Mercury's exosphere spatial distribution. The interpretation of Mercury's upper surface composition will therefore benefit by being related to Mercury's exospheric composition and density. Since loss to space occurs mainly via Mercury's exosphere its study will provide insight into Mercury's long-term evolution. Mercury's exosphere has been identified for a few decades as a marker of the Mercury–solar wind interaction. Understanding this interaction will allow exospheric observations to be a powerful remote method for monitoring this interaction. At the end, Mercury is also the best laboratory to measure and check the reality and efficiency of several processes of production of exospheric material, which are still debated and difficult to reproduce in laboratory. Such processes of ejection occur on almost every solid body in the Solar System especially on the Moon, and, therefore, any progress in our understanding will also benefit to the study of other planetary bodies.

References

Baker, D.N., 1990. Energy coupling in the magnetospheres of Earth and Mercury. Adv. Space Res. 10, (S)23–(S)26.

Barbieri, C., Benn, C.R., Cremonese, G., Verani, S., Zin, A., 2001. Meteor showers on the lunar atmosphere. EM&P 85, 479.

Barbieri, C., Verani, S., Cremonese, G., Sprague, A., Mendillo, M., Cosentino, R., Hunten, D., 2004. First observations of the Na exosphere of Mercury with the high resolution spectrograph of the 3.5 m Telescopio Nazionale Galileo. Planet. Space Sci. 52 (13), 1169–1175.

Benz, W., Slattery, W.L., Cameron, A.G.W., 1988. Collisional stripping of Mercury's atmosphere. Icarus 74, 516–528.

Betz, G., Wien, K., 1994. Energy and angular distributions of sputtered particles. Int. J. Mass Spectr. Ion Process. 140, 1–110.

Bida, T.A., Killen, R.M., Morgan, T.H., 2000. Discovery of calcium in Mercury's atmosphere. Nature 404, 159–161.

Blewett, D.T., Lucey, P.G., Hawke, B.R., Ling, G.G., Robinson, M.S., 1997. A comparison of Mercury reflectance and spectral quantities with those of the Moon. Icarus 129, 217–231.

Broadfoot, A.L., Kumar, S., Belton, M.J.S., McElroy, M.B., 1974. Mercury's atmosphere from Mariner 10: preliminary results. Science 185, 166–169.

Broadfoot, A.L., Shemansky, D.E., Kumar, S., 1976. Mariner 10: Mercury atmosphere. Geophys. Res. Lett. 3, 577–580.

Brown, M.E., 2001. Potassium in Europa's atmosphere. Icarus 151, 190–195.

Burbine, T.H., McCoy, T.J., Nittler, L.R., Benedix, G.K., Cloutis, E.A., Dickinson, T.L., 2002. Spectra of extremely reduced assemblages: Implications for Mercury. Meteoritics Planet. Sci. 37, 1233–1244.

Cassidy, T.A., Johnson, R.E., 2005. Monte Carlo model of sputtering and other ejection processes within a regolith. Icarus 176, 499–507.

Ceplecha, Z., 1992. Influx of interplanetary bodies onto Earth. Astron. Astrophys. 263, 361–366.

Chase, S.C., Miner, E.D., Morrison, D., Much, G., Neugebauer, G., 1976. Mariner 10 infrared radiometer result: temperatures and thermal properties of the surface of Mercury. Icarus 28, 655–678.

Cheng, A.F., Johnson, R.E., Krimigis, S.M., Lanzeroti, L.Z., 1987. Magnetosphere, exosphere, and surface of Mercury. Icarus 71, 430–440.

Christon, S.P., 1989. Plasma and energetic electron flux variations in Mercury 1 C event: evidence for a magnetospheric boundary layer. J. Geophys. Res. 94, 6481.

Cintala, M., 1992. Impact induced thermal effects in the lunar and Mercurian regoliths. J. Geophys. Res. 97, 947–973.

Cladis, J.B., Francis, W.E., Vondrak, R.R., 1994. Transport toward Earth of ions sputtered from the Moon's surface by the solar wind. J. Geophys. Res. 99 (A1), 53–64.

Colombo, G., 1965. Rotational period of the planet Mercury. Nature 208, 575.

Colombo, G., Shapiro, I.I., 1966. The rotation of the planet Mercury. Astrophys. J. 145, 296–307.

Connerney, J.E.P., Ness, N.F., 1988. Mercury's magnetic field and interior. In: Vilas, et al. (Eds.), Mercury. University of Arizona Press, Tucson, AZ, pp. 494–513.

Cooper, J.H., Johnson, R.E., Mauk, B.H., Gehrels, N., 2001. Energetic ion and electron irradiation of the icy Galilean satellites. Icarus 149, 133.

Cremonese, G., Verani, S., 1997. High resolution observations of the sodium emission from the Moon. Adv. Space Res. 19, 1561–1575.

Cremonese, G., Boehnhardt, H., Crovisier, J., Fitzsimmons, A., Fulle, M., Licandro, J., Pollacco, D., Rauer, H., Tozzi, G.P., West, R.M., 1997. Neutral sodium from comet Hale-Bopp: a third type of tail. Astrophys. J. Lett. 490, L199.

Cremonese, G., Bruno, M., Mangano, V., Marchi, S., Milillo, A., 2005. Release of neutral sodium from the surface of Mercury induced by meteoroid impacts. Icarus 177, 122–128.

Delcourt, D.C., Leblanc, F., 2005. Solar wind proton circulation inside Mercury's magnetosphere. Notes du Pôle de Planétologie de l'IPSL 12 ⟨http://www.ipsl.jussieu.fr/Documentation⟩.

Delcourt, D.C., Moore, T.E., Orsini, S., Milillo, A., Sauvaud, J.-A., 2002. Centrifugal acceleration of ions near Mercury. Geophys. Res. Lett. 29 (12).

Delcourt, D.C., Grimald, S., Leblanc, F., Bertherlier, J.-J., Millilo, A., Mura, A., 2003. A quantitative model of planetary Na^+ contribution to Mercury's magnetosphere. Ann. Geophys. 21, 1723–1736.

Fjeldbo, G., Kliore, A., Sweetnam, D., Esposito, P., Seidel, B., Howard, T., 1976. The occultation of Mariner 10 by Mercury. Icarus 29, 407–415.

Flynn, B., 1998. ORFEUS II far-ultraviolet observations of the lunar atmosphere. Astrophys. J. Lett. 500, L71–L74.

Flynn, B., Mendillo, M., 1993. A picture of the Moon's atmosphere. Science 261, 184–186.

Flynn, B.C., Stern, S.A., 1996. A spectroscopic survey of metallic species abundances in the lunar atmosphere. Icarus 124 (2), 530–536.

Goettel, K.A., 1988. Present bounds on the bulk composition of Mercury: Implications for planetary formation processes. In: Vilas, F., Chapman, C., Matthews, M. (Eds.), Mercury. University of Arizona Press, Tucson, AZ, pp. 613–621.

Gold, R.E., Solomon, S.C., McNutt Jr., R.L., Santo, A.G., Abshire, J.B., Acuna, M.H., Afzal, R.S., Anderson, B.J., Andrews, G.B., Bedini, P.D., Cain, J., Cheng, A.F., Evans, L.G., Feldman, W.C., Follas, R.B., Gloeckler, G., Goldsten, J.O., Hawkins, S.E., Izenberg, N.R., Jaskulek, S.E., Ketchum, E.A., Lankton, M.R., Lohr, D.A., Mauk, B.H., McClintock, W.E., Murchie, S.L., Schlemm, C.E., Smith, D.E., Starr, R.D., Zurbuchen, T.H., 2001. The MESSENGER mission to Mercury: mission payload. Planet. Space Sci. 49, 1467–1479.

Goldstein, B.D., Suess, S.T., Walker, R.J., 1981. Mercury: magnetospheric processes and the atmospheric supply and loss rate. J. Geophys. Res. 86, 5485–5499.

Hale, A.S., Hapke, B., 2002. A time-dependent model of radiative and conductive thermal energy transport in planetary regoliths with application to the Moon and Mercury. Icarus 156, 318–334.

Hapke, B., 2001. Space weathering from Mercury to the asteroid belts. J. Geophys. Res. 106 (E5), 10039–10074.

Harmon, J.K., Slade, M.A., 1992. Radar mapping of Mercury: full-disk images and polar anomalies. Science 258, 640–642.

Harmon, J.K., Slade, M.A., Velez, R.A., Crespo, A., Dryer, M.J., Johnson, J.M., 1994. Radar mapping of Mercury's polar anomalies. Nature 369, 213–215.

Hilchenbach, M., Hovestadt, D., Klecker, B., Mobius, E., 1991. Detection of singly ionized energetic lunar pick-up ions upstream of Earth's bow shock. In: Marsch, E., Schwenn, G. (Eds.), Solar Wind Seven. Pergamon, New York, pp. 150–155.

Hilchenbach, M., Hovestadt, D., Klecker, B., Mobius, E., 1993. Observation of energetic lunar pick-up ions near Earth. Adv. Space Res. 13 (10), 321–324.

Hodges, R.R., 1979. Methods for Monte Carlo simulation of the exospheres of the moon and Mercury. J. Geophys. Res. 85, 164–170.

Hodges, R.R., Hoffman, J.H., 1975. Implications of atmospheric Ar escape on the interior structure of the Moon. In: Proceedings of the Lunar Science Conference Sixth, pp. 3039–3047.

Hodges, R.R.J., Hoffman, J.H., Johnson, F.S., 1974. The lunar atmosphere. Icarus 21, 415–426.

Hood, L., Schubert, G., 1979. Inhibition of solar wind impingement on Mercury by planetary induction currents. J. Geophys. Res. 84, 2641–2647.

Huebner, W.F., Keady, J.J., Lyon, S.P., 1992. Solar photo rates for planetary atmospheres and atmospheric pollutants. Astrophys. Space Sci. 195, 1–294.

Hunten, D.M., Sprague, A.L., 1997. Origin and character of the lunar and Mercurian atmospheres. Adv. Space Res. 19 (10), 1551–1560.

Hunten, D.M., Sprague, A.L., 2002. Diurnal variation of Na and K at Mercury. Meteoritics Planet. Sci 37, 1165.

Hunten, D.M., Morgan, T.M., Shemansky, D.M., 1988. The Mercury atmosphere. In: Vilas, F., Chapman, C., Matthews, M. (Eds.), Mercury. University of Arizona Press, Tucson, AZ, pp. 562–612.

Hunten, D.M., Cremonese, G., Sprague, A.L., Hill, R.E., Verani, S., Kozlowski, R.W.H., 1998. The Leonid meteor shower and the lunar sodium atmosphere. Icarus 136, 298.

Ip, W.H., 1986. The sodium exosphere and magnetosphere of Mercury. Geophys. Res. Lett. 13, 423.

Ip, W.H., 1987. Mercury's magnetospheric irradiation effect on the surface. Geophys. Res. Lett. 14, 1191.

Ip, W.H., 1990. On solar radiation-driven surface transport of sodium atoms at Mercury. Astrophys. J. 356, 675–681.

Ip, W.-H., 1993. On the surface sputtering effects of magnetospheric charged particles at Mercury. Astrophys. J. 418, 451–456.

Ip, W.-H., 1997. Time-variable phenomena in the magnetosphere and exosphere of Mercury. Adv. Space. Res. 19, 1615.

Ip, W.-H., Kopp, A., 2002. MHD simulations of the solar wind interaction with Mercury. J. Geophys Res. 107 (A11), 1348.

Janhunen, P., Kallio, E., 2004. Surface conductivity of Mercury provides current closure and may affect magnetospheric symmetry. Ann. Geophys. 22, 1829–1837.

Jeanloz, R., Mitchell, D.L., Sprague, A.L., de Pater, I., 1995. Evidence for a basalt-free surface on Mercury and implications for internal heat. Science 268, 1455–1457.

Johnson, R.E., Baragiola, R., 1991. Lunar surface: sputtering and secondary ion mass spectroscopy. Geophys. Res. Lett. 18, 2169–2172.

Johnson, R.E., Quickenden, T.I., 1997. Photolysis and radiolysis of water ice on outer Solar System bodies. J. Geophys. Res. 102, 10985–10996.

Johnson, R.E., 1989. Application of laboratory data to the sputtering of a planetary regolith. Icarus 78, 206–210.

Johnson, R.E., 1990. Energetic Charged Particle Interactions with Atmospheres and Surfaces. Springer, Berlin.

Johnson, R.E., 2002. Surface boundary layer atmospheres. Chapter in Atmospheres in the Solar System: Comparative Aeronomy Geophysical Monograph 130, 203–219.

Jurac, S., Johnson, R.E., Baragiola, R.A., Sittler, E.C., 1995. Charging of ice grains by low-energy plasma? Application to Saturn's E ring. J. Geophys. Res. 100, 14,821–14,831.

Kabin, K., Gombosi, T.I., DeZeeuw, D.L., Powell, K.G., 2000. Interaction of Mercury with the solar wind. Icarus 143, 397–406.

Kallio, E., Janhunen, P., 2003a. Modelling the solar wind interaction with Mercury by a quasineutral hybrid model. Ann. Geophys. 21 (11), 2133–2145.

Kallio, E., Janhunen, P., 2003b. Solar wind and magnetospheric ion impact on Mercury's surface. Geophys. Res. Lett. 30 (17), 1877.

Kallio, E., Janhunen, P., 2004. The response of the Hermean magnetosphere to the interplanetary magnetic field. Adv. Space Res. 33, 2176–2181.

Killen, R., 2002. Source and maintenance of the Argon atmospheres of Mercury and the Moon. Meteoritics Planet. Sci. 37, 1223.

Killen, R.M., Ip, W.-H., 1999. The surface-bounded atmospheres of Mercury and the Moon. Rev. Geophys. 37, 361–406.

Killen, R.M., Morgan, T.H., 1993a. Maintaining the Na atmosphere of Mercury. Icarus 101, 293–312.

Killen, R.M., Morgan, T.H., 1993b. Diffusion of Na and K in the uppermost regolith of Mercury. J. Geophys. Res. 98, 23,589–23,601.

Killen, R.M., Benkhoff, J., Morgan, T.H., 1997. Mercury's polar caps and the generation of an OH exosphere. Icarus 125 (1), 195–211.

Killen, R.M., Potter, A.E., Fitzsimmons, A., Morgan, T.H., 1999. Sodium D2 line profiles: clues to the temperature structure of Mercury's exosphere. Planet. Space Sci., 471449–471458.

Killen, R.M., Potter, A.E., Reiff, P., Sarantos, M., Jackson, B.V., Hick, P., Giles, B., 2001. Evidence for space weather at Mercury. J. Geophys. Res. 106, 20,509–20,525.

Killen, R.M., Sarantos, M., Potter, A.E., Reiff, P.H., 2004. Source rates and ion recycling rates for Na and K in Mercury's atmosphere. Icarus, 1–19.

Killen, R.M., Bida, T.A., Morgan, T.H., 2005. The calcium exosphere of Mercury. Icarus 173, 3000–3311.

Kozlowski, R.W.H., Sprague, A.L., Hunten, D.M., 1990. Observations of potassium in the tenuous lunar atmosphere. Geophys. Res. Lett. 17 (12), 2253–2256.

Lammer, H., Bauer, J., 1997. Mercury's exosphere: origin of surface sputtering and implications. Planet. Space. Sci. 45, 73–79.

Lammer, H., Wurz, P., Patel, M.R., Killen, R., Kolb, C., Massetti, S., Orsini, S., Milillo, A., 2003. The variability of Mercury's exosphere by particle and radiation induced surface release processes. Icarus 166/2, 238–247.

Leblanc, F., Johnson, R.E., 2003. Mercury's sodium exosphere. Icarus 164, 261–281.

Leblanc, F., Luhmann, J.G., Johnson, R.E., Liu, M., 2003a. Solar energetic particle event at Mercury. Planet. Space Sci. 51, 339–352.

Leblanc, F., Delcourt, D., Johnson, R.E., 2003b. Mercury's sodium exosphere: Magnetospheric ion recycling. JGR-Planets 108 (E12), 5136.

Leblanc, F., Lammer, H., Torkar, K., Berthelier, J.J., Vaisberg, O., Woch, J., 2004. Ion of planetary origins at Mercury: some estimates. Notes du Pôle de Planétologie de l'IPSL 5 ⟨http://www.ipsl.jussieu.fr/Documentation⟩.

Ledlow, M.J., Burns, J.O., Gisler, G.R., Zhao, J.-H., Zeilik, M., Baker, D.N., 1992. Subsurface emission from Mercury: VLA observations at 2 and 6 cm. Astrophys. J. 384, 640–655.

Lewis, J.S., 1972. Metal silicate fractionation in the Solar System. Earth Planet. Sci. Lett. 15, 286–290.

Lewis, J., 1988. Origin and composition of Mercury. In: Vilas, F., Chapman, C.R., Matthews, M.S. (Eds.), Mercury. University of Arizona Press, Tucson, AZ.

Love, S.G., Brownlee, D.E., 1993. A direct measurement of the terrestrial mass accretion rate of cosmic dust. Science 262, 550–553.

Luhmann, J.G., Russell, C.T., Tsyganenko, N.A., 1998. Disturbances in Mercury's magnetosphere: Are Mariner 10 "substorms" simply driven? J. Geophys. Res. 103, 9113–9119.

Lukyanov, A.V., Barabash, S., Lundin, R., son Brandt, P.C., 2001. Energetic neutral atom imaging of Mercury's magnetosphere, 2: distribution of charged particles in a compact magnetosphere. Planet. Space Sci. 49, 1677–1684.

Lundin, R., Barabash, S., son Brandt, P.C., Eliasson, L., Nairn, C.M.C., Norberg, O., Sandahl, I., 1997. Ion acceleration processes in the Hermean and terrestrial magnetospheres. Adv. Space Res. 19, 1593.

Madey, T.E., Yakshinskiy, B.V., Ageev, V.N., Johnson, R.E., 1998. Desorption of alkali atoms and ions from oxide surfaces: relevance to origins of Na and K in atmospheres of Mercury and the Moon. J. Geophys. Res. 103 (E3), 5873–5887.

Madey, T.E., Johnson, R.E., Orlando, T.M., 2002. Far-out surface science: radiation-induced surface processes in the Solar System. Surf. Sci. 500, 838–858.

Mall, U., Kirsch, E., Cierpka, K., Wilken, B., Söding, A., Neubauer, F., Gloeckler, G., Galvin, A., 1998. Direct observation of lunar pick-up ions near the Moon. Geophys. Res. Lett. 25 (20), 3799–3802.

Manka, R.H., Michel, F.C., 1971. Lunar atmosphere as a source of Argon-40 and other lunar elements. In: Proceedings of the Lunar Science Conference Second, pp. 1717–1728.

Marchi, S., Morbidelli, A., Cremonese, G., 2005. Flux of meteoroid impacts on Mercury. Astron. Astrophys. 431, 1123–1127.

Massetti, S., Orsini, S., Milillo, A., Mura, A., De Angelis, E., Lammer, H., Wurz, P., 2003. Mapping of the cusp plasma precipitation on the surface of Mercury. Icarus 166, 229–237.

McGrath, M.A., Johnson, R.E., Lanzerotti, L.J., 1986. Sputtering of sodium on the planet Mercury. Nature 323, 694.

Mendillo, M., Baumgardner, J., 1995. Constraints on the origin of the Moon's atmosphere from observations during a lunar eclipse. Nature 377, 404–406.

Mendillo, M., Baumgardner, J., Flynn, B., 1991. Imaging observations of the extended sodium atmosphere of the Moon. Geophys. Res. Lett. 18, 2097–2100.

Mendillo, M., Baumgardner, J., Wilson, J., 1999. Observational test for the solar wind sputtering origin of the Moon's extended sodium atmosphere. Icarus 137, 13–23.

Molina-Cuberos, G.J., Witasse, O., Lebreton, J.-P., Rodrigo, R., Lopez-Moreno, J.J., 2003. Meteoritic ions in the atmosphere of Mars. Planet. Space Sci. 51, 239–249.

Morgan, T.H., Killen, R.M., 1997. A non-stochiometric model of the composition of the atmospheres of Mercury and the Moon. Planet. Space Sci. 45, 81.

Morgan, T.H., Shemansky, D.E., 1991. Limits to the lunar atmosphere. J. Geophys. Res. 96, 1351–1367.

Morgan, T.H., Zook, H.A., Potter, A.E., 1988. Impact-driven supply of sodium and potassium to the atmosphere of Mercury. Icarus 75, 156–170.

Morgan, T.H., Zook, H.A., Potter, A.E., 1989. Production of sodium vapor from exposed regolith in the inner Solar System. In: Proceedings of the Lunar Planetary Science Conference, vol. 19, 297–304.

Mura, A., Orsini, S., Milillo, A., Delcourt, D., Massetti, S., De Angelis, E., 2005. Dayside H^+ circulation at Mercury and neutral particle emission. Icarus 175, 305–319.

Nash, D.B., Matson, D.L., Johnson, T.V., Fanale, F.P., 1975. Na-D line emission from rock specimens by proton bombardment: implications for emissions from Jupiter's satellite Io. J. Geophys. Res. 80, 1875–1879.

Ness, N.F., Behannon, K.W., Lepping, R.P., Whang, Y.C., Schatten, K.H., 1974. Magnetic field observations near Mercury: preliminary results from Mariner 10. Science 185, 151.

Ness, N.F., Behannon, K.W., Lepping, R.P., Whang, Y.C., 1975. The magnetic field of Mercury, 1. J. Geophys. Res. 80, 2708–2716.

O'Keefe, J.D., Ahrens, T.J., 1977. Impact induced energy partitioning, melting, and vaporization on terrestrial planets. Lunar Planet. Sci. 8, 3357–3374.

Ogilvie, K.W., Scudder, J.D., Vasyliunas, V.M., Hartle, R.E., Siscoe, G.L., 1977. Observations at the planet Mercury by the plasma electron experiment: Mariner 10. J. Geophys Res. 82, 1807–1824.

Parker, J.Wm., Stern, S.A., Gladstone, G.R., Shull, J.M., 1998. The spectroscopic detectability of Argon in the lunar atmosphere. Astrophys. J. 509, L61–L64.

Pierazzo, E., Melosh, H.J., 1999. Hydrocode modeling of Chicxulub as an oblique impact event. Earth Planet. Sci. Lett. 165, 163.

Potter, A.E., 1995. Chemical sputtering could produce sodium vapor and ice on Mercury. Geophys. Res. Lett. 22, 3289–3292.

Potter, A.E., Morgan, T.H., 1985. Discovery of sodium in the atmosphere of Mercury. Science 229, 651–653.

Potter, A.E., Morgan, T.H., 1986. Potassium in the atmosphere of Mercury. Icarus 67, 336–340.

Potter, A.E., Morgan, T.H., 1987. Variation of sodium on Mercury with solar radiation pressure. Icarus 71, 472–477.

Potter, A.E., Morgan, T.H., 1988. Discovery of sodium and potassium vapor in the atmosphere of the Moon. Science 241, 675–680.

Potter, A.E., Morgan, T.H., 1990. Evidence for magnetospheric effects on the sodium atmosphere of Mercury. Science 248, 835.

Potter, A.E., Morgan, T.H., 1997a. Sodium and potassium atmospheres of Mercury. Planet. Space Sci. 45 (1), 95–100.

Potter, A.E., Morgan, T.H., 1997b. Evidence for suprathermal sodium on Mercury. Adv. Space Res. 19 (10), 1571–1576.

Potter, A.E., Morgan, T.H., Killen, R.M., 1999. Rapid changes in the sodium exosphere of Mercury. Planet. Space Sci. 47, 1441–1448.

Potter, A.E., Killen, R.M., Morgan, T.H., 2002a. The sodium tail of Mercury. Meteoritic and Planetary Science 37, 1165–1172.

Potter, A.E., Anderson, C.M., Killen, R.M., Morgan, T.H., 2002b. Ratio of sodium to potassium in the Mercury exosphere. J. Geophys. Res. 107 (E6), doi:10.1029/2000JE001493.

Potter, A.E., Killen, R.M., Sarantos, M., 2006. Spatial distribution of sodium on Mercury. Icarus 181, 1–12.

Roth, J., 1983. Chemical sputtering. In: Gehrisch, R. (Ed.), Sputtering by Particle Bombardment II, Topics in Applied Physics, vol. 52. Springer, Berlin, pp. 91–145.

Russell, C.T., Baker, D.N., Slavin, J.A., 1988. The magnetosphere of Mercury. In: Vilas, F., Chapman, C., Matthews, M. (Eds.), Mercury. University of Arizona Press, Tucson, pp. 514–561.

Santo, A.G., Gold, R.E., McNutt, R.L., Solomon, S.C., Ercol, C.J., Farquhar, R.W., Hartka, T.J., Jenkins, J.E., McAdams, J.V., Mosher, L.E., Persons, D.F., Artis, D.A., Bokulic, R.S., Conde, R.F., Dakermanji, G., Goss, M.E., Haley, D.R., Heeres, K.J., Maurer, R.H., Moore, R.C., Rodberg, E.H., Stern, T.G., Wiley, S.R., Williams, B.G., Yen, C.L., Peterson, M.R., 2001. The MESSENGER mission to Mercury: spacecraft and mission design. Planet. Space Sci. 49, 1481–1500.

Sarantos, M., Reiff, P.H., Hill, T.W., Killen, R.M., Urquhart, A.L., 2001. A Bx-interconnected magnetosphere model for Mercury. Planet. Space Sci. 49, 1629–1635.

Schleicher, H., Wiedemann, G., Wöhl, H., Berkefeld, T., Soltau, D., 2004. Detection of neutral sodium above Mercury during the transit on 2003 May 7. A&A 425, 1119–1124.

Shemansky, D.E., Broadfoot, A.L., 1977. Interaction of the surfaces of the Moon and Mercury with their exospheric atmospheres. Rev. Geophys. 15, 491–499.

Shemansky, D.E., Morgan, T.H., 1991. Source processes for the alkali metals in the atmosphere of Mercury. Geophys. Res. Lett. 18, 1659–1662.

Simpson, J.A., Eraker, J.H., Lamport, J.E., Walpole, P.H., 1974. Electrons and protons accelerated in Mercury's magnetic field. Science 185, 160.

Siscoe, G.L., Christofer, L., 1975. Variations in the solar wind standof distance at Mercury. Geophys. Res. Lett. 2, 158.

Siscoe, G.L., Ness, N.F., Yeates, C.M., 1975. Substorms on Mercury? J. Geophys. Res. 80, 4359.

Slade, M.A., Butler, B.J., Muhleman, D.O., 1992. Mercury radar imaging: evidence for polar ice. Science 258, 635–640.

Slavin, J.A., Owen, J.C.J., Connerney, J.E.P., Christon, S.P., 1997. Mariner 10 observations of field-aligned currents at Mercury. Planet. Space Sci. 45, 133–141.

Smith, R.S., Kay, B.D., 1997. Adsorption, desorption and crystallization kinetics in nanoscale water films. Recent Res. Dev./Phys. Chem. 1, 209–219.

Smith, S.M., Wilson, J.K., et al., 1999. Discovery of the distant Lunar sodium tail and its enhancement following the Leonid Meteor shower of 1998. Geophys. Res. Lett. 26, 1642–1652.

Smith, G.R., Shemansky, D.E., Broadfoot, A.L., Wallace, L., 1978. Monte Carlo modeling of exospheric bodies: Mercury. J. Geophys. Res. 83, 3783–3790.

Smyth, W.H., 1986. Nature and variability of Mercury's sodium atmosphere. Nature 323, 696–699.

Smyth, W.H., Marconi, M.L., 1995. Theoretical overview and modeling of the sodium and potassium atmospheres of Mercury 441, 839–864.

Solomon, S.C., McNutt, R.L., Gold, R.E., Acuna, M.H., Baker, D.N., Boynton, W.V., Chapman, C.R., Cheng, A.F., Gloeckler, G., Head, J.W., Krimigis, S.M., McClintock, W.E., Murchie, S.L., Peale, S.J., Phillips, R.J., Robinson, M.S., Slavin, J.A., Smith, D.E., Strom, R.G., Trombka, J.I., Zuber, M.T., 2001. The MESSENGER mission to Mercury: scientific objectives and implementation. Planet. Space Sci. 49, 1445–1465.

Soter, S., Ulrichs, J., 1967. Rotation and heating of the planet Mercury. Nature 214, 1315–1316.

Speiser, T.W., 1965. Particle trajectory in model current sheets, 1: analytical solutions. J. Geophys. Res. 70, 4219.

Spohn, T., Sohl, F., Wieczerkowski, K., Conzelmann, V., 2001. The interior structure of Mercury: what we know, what we expect from BepiColombo. Planet. Space Sci. 49, 1561–1570.

Sprague, A.L., 1990. A diffusion source for sodium and potassium in the atmospheres of Mercury and the Moon. Icarus 84, 93–105.

Sprague, A.L., 1992. Mercury's atmospheric bright spots and Potassium variations: a possible cause. J. Geophys. Res. 97, 18257.

Sprague, A.L., 1993. A correction to Mercury's atmospheric sodium bright spots and potassium variations: a possible cause. J. Geophys. Res. 98 (E1), 1231.

Sprague, A.L., Kozlowski, R.W.H., Hunten, D.M., 1990. Caloris Basin: an enhanced source for potassium in Mercury's atmosphere. Science 249, 1140–1143.

Sprague, A.L., Kozlowski, R.W.H., Hunten, D.M., Wells, W.K., Grosse, F.A., 1992. The sodium and potassium atmosphere of the Moon and its interaction with the surface. Icarus 96, 27–42.

Sprague, A.L., Kozlowski, R.W.H., Witteborn, F.C., Cruikshank, D.P., Wooden, D.H., 1994. Mercury: Evidence for anorthosite and basalt from mid-infrared (7.5–13.5 micrometers) spectroscopy. Icarus 109, 156–167.

Sprague, A.L., Hunten, D.M., Lodders, K., 1995. Sulfur at Mercury, elemental at the poles and sulfides in the regolith. Icarus 118, 211.

Sprague, A.L., Hunten, D.M., Lodders, K., 1996a. Erratum: sulfur at Mercury, elemental at the poles and sulfides in the regolith. Icarus 123, 123.

Sprague, A.L., Hunten, D.M., Grosse, F.A., 1996b. Upper limit for lithium in Mercury's atmosphere. Icarus 123, 345–349.

Sprague, A.L., Kozlowski, R.W.H., Hunten, D.M., Schneider, N.M., Domingue, D.L., Wells, W.K., Schmitt, W., Fink, U., 1997a. Distribution and abundance of sodium in Mercury's atmosphere, 1985–1988. Icarus 129, 506–527.

Sprague, A.L., Nash, D.B., Witteborn, F.C., Cruikshank, D.P., 1997b. Mercury's feldspar connection mid-IR measurements suggest plagioclase. Adv. Space Res. 19, 1507–1510.

Sprague, A.L., Schmitt, W.J., Hill, R.E., 1998a. Mercury: sodium atmospheric enhancements, radar bright spots and visible surface features. Icarus 135, 60.

Sprague, A.L., Hunten, D.M., Kozlowski, R.W., Grosse, F.A., Hill, R.E., Morris, R.L., 1998b. Observations of sodium in the lunar atmosphere during international lunar atmosphere week, 1995. Icarus 131, 372–381.

Stern, S.A., 1999. The lunar atmosphere: history, status, current problems and context. Rev. Geophys. 37 (4), 453–491.

Stern, S.A., Flynn, B.C., 1995. Narrow-field imaging of the lunar sodium exosphere. Astron. J. 109, 835–841.

Stern, S.A., Parker, J.W., Morgan, T.H., Flynn, B.C., Hunten, D.M., Sprague, A.L., Mendillo, M., Festou, M.C., 1997. An HST search for magnesium in the lunar atmosphere. Icarus 127, 523–526.

Stirniman, M.J., Huang, C., Smith, R.Scott, Joyce, S.A., Kay, Bruce D., 1996. The adsorption and desorption of water on single crystal MgO(100): the role of surface defects. J. Chem. Phys. 105 (3), 1295–1298.

Stubbs, T.J., Vondrak, R.R., Farrell, W.M., 2005. A dynamic fountain model for lunar dust. In: Proceedings of the Lunar Science Conference 36th, p. 1899.

Sugita, S., Schultz, P.H., Adams, M.A., 1998. Spectroscopic measurements of vapor clouds due to oblique impact. J. Geophys. Res. 103, 19427–19441.

Tyler, A.L., Kozlowski, R.W.H., Hunten, D.M., 1988. Observations of sodium in the tenuous lunar atmosphere. Geophys. Res. Lett. 15, 1141–1144.

Verani, S., Barbieri, C., Benn, C., Cremonese, G., 1998. Possible detection of meteor stream effects on the lunar sodium atmosphere. Planet. Space Sci. 35, 1003–1006.

Verani, S., Barbieri, C., Benn, C.R., Cremonese, G., Mendillo, M., 2001. The 1999 Quadrantids and the lunar Na atmosphere. MNRAS 327, 244.

Warell, J., Blewett, D.T., 2004. Properties of the Hermean regolith: V. New optical reflectance spectra, comparison with lunar anorthosites, and mineralogical modelling. Icarus, 168.

Wasson, J.T., 1988. The building stones of the planets. In: Vilas, F., Chapman, C.R., Matthews, M.S. (Eds.), Mercury. The University of Arizona Press, Tucson, AZ, London.

Watters, T.R., Prinz, M., 1979. Aubrites: their origin and relationship to enstatite chondrites. In: Proceedings of the Lunar Planetary Science Conference 10th, pp. 1073–1093.

Wetherill, G.W., 1988. Accumulation of Mercury from planetesimals. In: Vilas, F., Chapman, C.R., Matthews, M.S. (Eds.), Mercury. University of Arizona Press, Tucson, AZ, pp. 670–691.

Wilson, J., Smith, S.M., Baumgardner, J., Mendillo, M., 1999. Modeling an enhancement of the lunar sodium atmosphere and tail during the Leonid meteor shower of 1998. Geophys. Res. Lett. 26, 1649.

Wilson, J.K., Baumgardner, J., Mendillo, M., 2003. The outer limits of the lunar sodium exosphere. Geophys. Res. Lett. 30 (51–1), 1649.

Wilson, J.K., Mendillo, M., Spence, H., 2005. Magnetospheric influence on the Moon's exosphere. J. Geophys. Res., submitted for publication.

Yakshinskiy, B.V., Madey, T.E., 2000. Desorption induced by electronic transition of Na from SiO_2: relevance to tenuous planetary atmospheres. Surf. Sci. 451, 160–165.

Yakshinskiy, B.V., Madey, T.E., 2001. Electron and photon-stimulated desorption of K from an ice surface. J. Geophys. Res. 106, 33303–33308.

Yakshinskiy, B.V., Madey, T.E., Ageev, V.N., 2000. Thermal desorption of sodium atoms from thin SiO_2 films. Surf. Rev. Lett. 7, 75–87.

Yan, N., Chassefière, E., Sarkissian, A., Leblanc, F., 2006a. Thermal model of Mercury's surface and subsurface: Impact of subsurface physical heterogeneities on the surface temperature. Adv. Space Res. 38 (4), 583–588.

Yan, N., Leblanc, F., Chassefière, E., 2006b. Potential relations between Caloris Basin and Mercury's sodium exosphere. Icarus 181, 348–362.

Yashinskiy, B.V., Madey, T.E., 1999. Photon-stimulated desorption as a substantial source of sodium in the lunar atmosphere. Nature 400, 642–644.